ACS POLYMERS Au
AN OPEN ACCESS JOURNAL OF THE AMERICAN CHEMICAL SOCIETY

pubs.acs.org/polymerau

Perspective

Dynamics and Equilibration Mechanisms in Block Copolymer Particles

Timothy P. Lodge,* Claire L. Seitzinger, Sarah C. Seeger, Sanghee Yang, Supriya Gupta, and Kevin D. Dorfman

Cite This: *ACS Polym. Au* 2022, 2, 397–416

Read Online

ACCESS | Metrics & More | Article Recommendations

ABSTRACT: Self-assembly of block copolymers into interesting and useful nanostructures, in both solution and bulk, is a vibrant research arena. While much attention has been paid to characterization and prediction of equilibrium phases, the associated dynamic processes are far from fully understood. Here, we explore what is known and not known about the equilibration of particle phases in the bulk, and spherical micelles in solution. The presumed primary equilibration mechanisms are chain exchange, fusion, and fragmentation. These processes have been extensively studied in surfactants and lipids, where they occur on subsecond time scales. In contrast, increased chain lengths in block copolymers create much larger barriers, and time scales can become prohibitively slow. In practice, equilibration of block copolymers is achievable only in proximity to the critical micelle temperature (in solution) or the order–disorder transition (in the bulk). Detailed theories for these processes in block copolymers are few. In the bulk, the rate of chain exchange can be quantified by tracer diffusion measurements. Often the rate of equilibration, in terms of number density and aggregation number of particles, is much slower than chain exchange, and consequently observed particle phases are often metastable. This is particularly true in regions of the phase diagram where Frank–Kasper phases occur. Chain exchange in solution has been explored quantitatively by time-resolved SANS, but the results are not well captured by theory. Computer simulations, particularly via dissipative particle dynamics, are beginning to shed light on the chain escape mechanism at the molecular level. The rate of fragmentation has been quantified in a few experimental systems, and TEM images support a mechanism akin to the anaphase stage of mitosis in cells, via a thin neck that pinches off to produce two smaller micelles. Direct measurements of micelle fusion are quite rare. Suggestions for future theoretical, computational, and experimental efforts are offered.

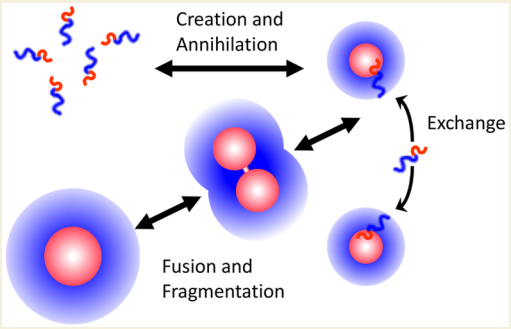

KEYWORDS: *block copolymer, micelle, chain exchange, fragmentation, fusion, Frank–Kasper phase, kinetics*

I. INTRODUCTION AND SCOPE

Block copolymer (BCP) self-assembly is a versatile route to nanostructured materials, both in solution[1−4] and bulk.[5] Advances in controlled polymerization have enabled a rich palette of monomers to be readily enchained into di-, tri-, and multiblock architectures. Concurrently, theoretical approaches have built an impressive ability to predict equilibrium structures, primarily in terms of block degrees of polymerization (N) and interaction parameter (χ). For example, self-consistent field theory can discriminate among delicately poised competing nanostructures in the bulk,[6−9] including the recently discovered Frank–Kasper (FK) phases.[10−14] In solution, equilibrium micellar structures have in principle been understood for some time, initially by scaling arguments[15−18] and then more quantitatively.[19−22] The same free energy competition dictates structure in both cases, namely the entropy penalty for chain stretching versus the energy penalty of forming an interface; however, the packing of chains into micelles in solution is not subject to a space-filling constraint, and consequently diblock amphiphiles overwhelmingly form spheres, worms, and vesicles (polymersomes). Such nanostructures are of immense interest across a broad spectrum of applications, including viscosity modification for motor oil, drug and gene delivery vehicles, imaging and contrast agents, nanoreactors, and food and agricultural formulations.[23−27]

While the *equilibrium* packing in self-assembled BCPs is relatively well understood, the *dynamic* processes by which such structures evolve are not.[28] Among the complicating issues are the roles of (a) energetic barriers for one block to pass through domains rich in the other or through a poor solvent; (b) strongly temperature- and composition-dependent

Received: July 2, 2022
Revised: August 10, 2022
Accepted: August 10, 2022
Published: August 23, 2022

segmental dynamics (typically tied to the glass transition, which is likely spatially inhomogeneous); and (c) the extent of entanglement of the (inherently) tethered blocks. These phenomena are relevant for all concentration regimes, but for micelles in solution, and with suitably chosen core blocks, the energetic barriers are the primary concern. While BCP micelles share many attributes with low molar mass surfactant and lipid analogs,[29,30] one key difference is that the former are much more likely to be nonequilibrium structures. The primary obstacle is readily identified. For a nonionic surfactant, it costs just over 1 k_BT to drag each $-CH_2-$ group into water.[29] For a C_{10} alkyl tail, the resulting barrier $E \approx 11\ k_BT$ is readily overcome, but for a C_{20} surfactant, rapid equilibration becomes an issue.[31] In BCPs, the number of repeat units in the core block, N_{core}, is more typically in the range of 10^2-10^3. While the energy penalty per repeat unit (i.e., χ) can be made much smaller by choosing a less-selective solvent than water, it is still common to encounter a barrier to chain escape $E \gg 10-20\ k_BT$. This barrier is also strongly dependent on N_{core}, as will be discussed in detail. The same argument also rationalizes a very small concentration of free chains, and an anticipated critical micelle concentration (CMC) that is typically too low to detect. Furthermore, chain escape and exchange between micelles is *necessary* to achieve equilibrium in general, but is usually far from *sufficient*.

In this Perspective, we will restrict our focus to nominally spherical particles; Figure 1 presents a cartoon of the various

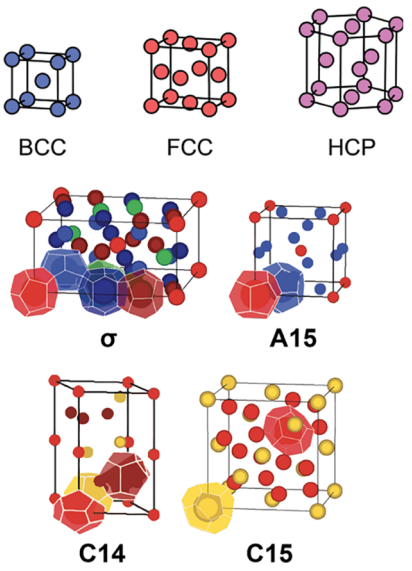

Figure 1. Schematic representation of known packings of nominally spherical particles of BCPs in the bulk.[32] These include the most prevalent body-centered cubic (BCC) and two close-packed phases: face-centered cubic (FCC) and hexagonally close-packed (HCP). In these three phases, all particles are equivalent. In the σ, A15, C14, and C15, phases, however, there are 5, 2, 3, and 2 distinct particle sizes, respectively, as indicated by the shaded Wigner–Seitz cells.

structures of interest in the melt.[32] These correspond to materials that self-assemble into body-centered cubic (BCC), face-centered cubic (FCC), hexagonally close-packed (HCP), and the various Frank–Kasper phases (particularly σ, A15, C14, and C15). However, some comparisons will be drawn with lamellar (LAM), hexagonal (HEX), and network phases, such as double gyroid (GYR). In solution, we will focus on "classical" core–corona spherical micelles, with some remarks about worm-like micelles and vesicles. We will also confine the discussion to AB diblock copolymers, with a few references to ABA triblocks. The principles discussed can certainly be extended to ABC terpolymers and to other, more elaborate architectures. We will also assume very narrowly distributed polymers in terms of composition and molar mass, recognizing that in some circumstances dispersity can play an important role in stabilizing one ordered phase over another. We will define the core- and corona-forming block volumetric degrees of polymerization as N_{core} and N_{corona}, respectively. In the bulk, the relevant interaction parameter is χ_{AB}; in solution, it is χ_{AS} between the core block and the solvent that drives micellization. However, χ_{AB} can still play a role; the combined effects of both interactions can be subsumed in an interfacial energy, γ, at the surface of the core. The key characteristic of a spherical particle is the mean aggregation number Q, and its distribution; the equilibrium value, Q_{eq}, depends on the relevant χ or γ, and is therefore a function of temperature, T. The (in)ability of Q to adjust to changes in T often determines whether a particle system can equilibrate.

II. OVERVIEW OF EQUILIBRATION MECHANISMS

Figure 2 provides an illustration of the canonical mechanisms of micelle equilibration. These include *creation*, in which chains

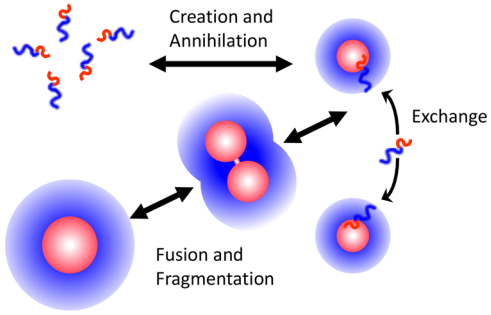

Figure 2. Schematic cartoon of five equilibration processes discussed in the text

or small clusters of chains nucleate and grow into a new micelle; *annihilation*, whereby a cascade of exchange and/or fragmentation and fusion events eliminates one micelle; *chain exchange*, in which an individual molecule escapes from one aggregate, diffuses through the medium, and inserts into a different particle; *fragmentation*, or *fission*, in which a particle spontaneously divides into two (or more) smaller micelles; *fusion*, in which two (or more) micelles merge into one. Note that a fragmentation event could create "daughter" micelles of quite different sizes, Q_1 and Q_2; in the limit that $Q_1 \to 1$, chain exchange can be seen as a subset of fragmentation and fusion.

The kinetics of these processes were first modeled in detail for surfactants by Aniansson, Wall, and co-workers.[33−35] Subsequent experimental studies for surfactants and some BCPs (Pluronics, in particular) have confirmed many aspects of this picture;[36−39] much of the pioneering work has been summarized in detail by Zana.[30] In this approach surfactants are pictured as falling into three states: single molecules, or very small aggregates (oligomers); "proper" micelles, with a core–shell structure; and a small population of intermediate aggregates. The system responds to a perturbation in two stages. The first, relatively rapid process, corresponds to

https://doi.org/10.1021/acspolymersau.2c00033
ACS Polym. Au 2022, 2, 397−416

surfactant exchange, whereas the slower one relies on reaching a new equilibrium between micelles and oligomers, mediated by stepwise association/dissociation of single surfactants with intermediate aggregates. As the population of the aggregates is so low, this step is slow. Also, as fusion relies on encounters between two aggregates, it was assumed to be negligible (at least at low overall surfactant concentrations). For BCP micelles, the first detailed dynamical theory was proposed by Halperin and Alexander;[40,41] they emphasized chain exchange, arguing that neither fusion nor fragmentation were probable, at least when close to equilibrium. Dormidontova took a broader view,[42] and offered scaling predictions for all three processes, and their relative contributions under different conditions. Nyrkova and Semenov focused on creation and annihilation processes, and especially the response to abrupt changes in conditions (e.g., temperature).[43] Of particular relevance is their prediction that large barriers could exist for both of these processes, even when the overall process was strongly favored, and that experimentally one might find micellization only observed at a *critical aggregation concentration* (CAC) far above the expected *critical micelle concentration* (CMC). They also called into question some of Dormidontova's results.

II.A. Creation/Annihilation

While most of the work on micelle dynamics focuses on equilibration of already-formed micelles, it is also interesting to consider their creation and annihilation. Block copolymer micelle creation from free amphiphiles is expected to be a rather chaotic process. The theoretical framework is the extended Aniansson−Wall−Teubner−Kahlweit model.[44,45,33] Two processes are proposed—one faster, where individual chains associate and dissociate from each other, and one slower, where aggregates of chains encounter one another and fuse into micelles. This behavior is comparable to the understanding of the creation of surfactant micelles. Kahlweit and Teubner discuss a variety of detection methods for analyzing micelle formation in surfactants.[44] Specific electrical conductivity can be used to track micellization in the ionic case. Below the CMC, the solute behaves like a strong electrolyte. However, at the CMC, a new species appears, which behaves more like a weak electrolyte. Ultrasonic absorption is caused by pressure-induced volume change, and only the fast relaxation process can be detected, specifically ones that are accompanied by a volume change and therefore a change of the monomer concentration.[46]

Far away from the CMC or CMT, micellization is typically too rapid to be studied experimentally. Honda and co-workers chose poly(α-methylstyrene)-*b*-poly(vinylphenethyl alcohol) in benzyl alcohol, which has a CMT just above room temperature.[47] They used time-resolved light scattering to follow micellization, and compared the apparent molecular weight and radius of gyration to determine whether growth of micelle size or aggregation number dominates. They determined that first the number of micelles increases until the unimer concentration is quite low, at which point chain expulsion/insertion increases the overall size of the micelles but decreases the number of micelles. This interpretation assumes, therefore, that some micelles completely disappear. More recently, Jensen and co-workers used a stopped-flow small-angle X-ray scattering method to study formation of surfactant micelles.[48] They used a system of dodecyl maltoside (DDM) in dimethylformamide (DMF) and added water to induce micellization. The micelles formed and grew by stepwise insertion/expulsion of single surfactant molecules; they did not see evidence for premicellar aggregates as evidence of fusion/fragmentation in their system. Lund and co-workers took a similar approach with block copolymers, and used poly(ethylene-*alt*-propylene)-*b*-poly(ethylene oxide) (PEP-PEO) in water/DMF solvent mixtures.[49] With the stopped-flow SAXS apparatus, they observed a two-step association, of primary micellization followed by unimer exchange (Figure 3). Their results are in broad agreement with the Aniansson−Wall mechanism.

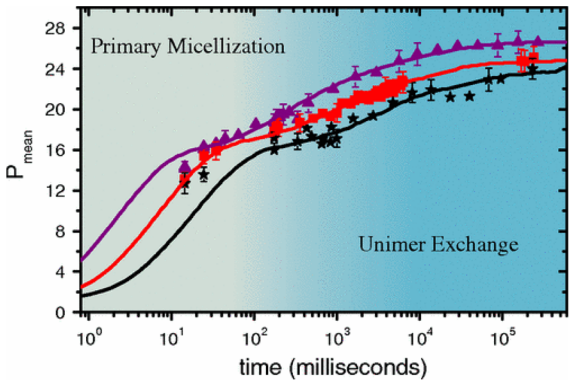

Figure 3. Time dependence of the mean aggregation number, P_{mean}, detailing the two-step nature of the formation of micelles, reproduced with permission from ref 49. Copyright 2009 American Physical Society.

Micelle annihilation has also been studied. Kreshek et al. used temperature-jump spectrophotometric studies of dodecylpyridinium iodide surfactant micelles in aqueous solution to determine the rate of dissociation.[50] They found that, slightly above the CMC, both the fast step and a subsequent slow step can be observed in kinetic measurements. Far above the CMC, only a slow step is observed, and below the CMC, only the fast step is observed. In this case, the "slow step" is a relaxation process because of an imbalance in the unimer/micelle equilibrium with a temperature perturbation, while the "fast step" is because of the perturbation of the ion pair and charge transfer equilibrium. Theoretical treatment of annihilation by Nyrkova and Semenov predicts that dissociation depends on the concentration of unimers, not that of micelles.[43] When the unimer concentration is above that of a critical dissociation concentration, annihilation will be slow. These predictions have not been extensively examined experimentally.

II.B. Micelle Preparation Routes

As will be emphasized throughout, BCP micelles are often far from equilibrium, because the solvophobic block is long, and the product χN_{core} is large. Consequently, the critical micelle concentration (CMC) is very small, and almost always experimentally inaccessible, that is, in the vicinity of the CMC the analytical signal is too low to measure reliably. This strong segregation presents a challenge in terms of how to prepare micelles at finite concentrations, a challenge that is rarely present for surfactants. Several strategies have been adopted, each with its accompanying advantages and disadvantages. One approach is direct dissolution, where the copolymer and the solvent are mixed, stirred, and possibly heated. This can be time-consuming and is not viable if the core block has a high T_g, such as polystyrene (PS) or poly(methylmethacrylate) (PMMA). It is also worth noting

https://doi.org/10.1021/acspolymersau.2c00033
ACS Polym. Au 2022, 2, 397−416

that, in most cases, the bulk copolymer is in the ordered state. A variant of direct dissolution that can exploit this fact is to cast a thin copolymer film from a volatile good solvent. Then, exposure to the desired selective solvent can result in penetration into the ordered corona block domains, followed by pinching off into spherical micelles. In some cases this approach can yield a relatively narrow distribution of initial micelle sizes, which can be useful; of course, a narrow micelle size distribution by itself says nothing about how far the aggregation number may be from equilibrium. An alternate approach is to use a volatile cosolvent. This is particularly convenient for nonvolatile or high boiling point target solvents, such as ionic liquids[51] or hydrocarbon oils.[52] In this approach, the resulting micelle size is often smaller than the equilibrium value, because micelles are first formed at some critical cosolvent content; further removal of cosolvent increases the interfacial tension but the aggregation number may not be able to grow rapidly enough to keep pace. A related approach is to slowly add a BCP solution in a cosolvent dropwise to a bath of the target solvent, such as water. Micelles appear immediately upon mixing, and the relatively small amount of cosolvent can be removed by dialysis. Under favorable circumstances, it is possible to go directly from a BCP solution to a micellar solution by a change in temperature, if the core-forming block has an accessible theta temperature. Examples have reported, for both upper critical and lower critical solution behavior, that is, micelles form on cooling or heating, respectively.[2,53,54] These transition temperatures may be designated as upper and lower critical micelle temperatures, UCMT and LCMT, respectively. However, one consequence of the general inaccessibility of a homogeneous solution of block copolymers is that it is difficult to study the kinetics of BCP micelle formation from an initially homogeneous state.

Once BCP micelles have been prepared, how close to the CMT must one be to enable equilibration of Q on a reasonable time scale? An example is provided in Figure 4, where

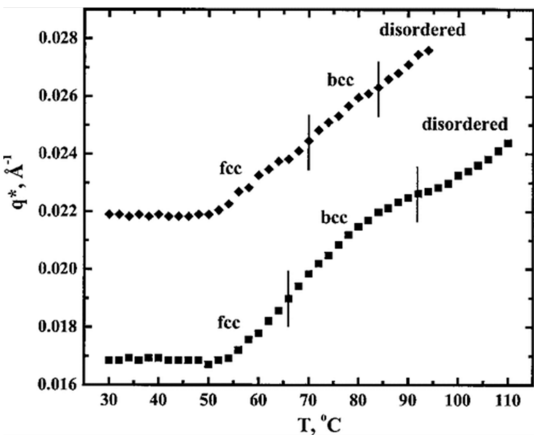

Figure 4. Primary peak position from SAXS measurements of 15% perdeuterated PS-PI (15−15) in tetradecane (lower trace), and 25% PS-perdeuterated PI (15−15) in diethyl phthalate (upper trace) versus temperature. Both solutions transition from a disordered solution of micelles to a BCC phase, and then to an FCC packing; the monotonic decrease in q^* reflects increasing segregation and growth of micelle aggregation number, Q, with cooling in these UCMT systems. However, both systems depart from equilibrium near 50 °C. Reproduced with permission from ref 55. Copyright 2009 American Physical Society.

symmetric polystyrene-*b*-polyisoprene (PS-PI) BCPs with total $M \approx 30\,000$ kDa were directly dissolved at high temperature in a PS-selective solvent, diethyl phthalate, and a PI-selective solvent, tetradecane.[55,56] In each case the core block was perdeuterated, to enable detailed characterization by small-angle neutron scattering (SANS). The primary peak position, q^*, from SAXS is shown as a function of temperature upon slow cooling. At high temperatures the micelles are sufficiently small and few in number, but near 90 °C the micelles grow and impinge upon one another, and pack onto a BCC lattice below an order−disorder transition. Further cooling leads to the expected increase in Q and a corresponding decrease in the unit cell size, such that a BCC to FCC order−order transition emerges. Then, around 50 °C, both systems depart from equilibrium, as q^* remains fixed. Importantly, this occurs in both systems, and therefore reflects a thermodynamic barrier; the two different micellar cores have T_gs that differ by almost 200 °C, so that is not the origin of the onset of nonergodicity. Detailed analysis of these data is complicated by the fact that the amount of solvent in the micelle core is also a smoothly decreasing function of temperature, with the cores becoming almost "dry" near room temperature (based on SANS measurements with labeled solvent).[56]

III. EQUILIBRATION OF PARTICLE PHASES IN THE MELT

There are two aspects to this process. One is chain exchange, which can be captured by measurements of tracer diffusion. The other is changing the number density of micelles, for which chain exchange is not sufficient. The long-range diffusion of individual chains in ordered block copolymer melts has been studied experimentally for a variety of chemical systems and ordered structures.[57−67] For sphere phases, it is sufficient to consider a single isotropic tracer diffusivity D. For lamellae, hexagonally packed cylinders, and network phases such as the double gyroid, two distinct diffusivities apply: one parallel to the interdomain interfaces, D_{par}, and one perpendicular, D_{perp}. The latter corresponds to D for particle phases, such as those shown in Figure 1. In all cases, one can express the diffusivity in terms of a "bare" value, D_0, which reflects the hypothetical value for an equivalent molecule (in terms of N, monomeric friction, ζ, and degree of entanglement) but in the absence of nanostructure, and a barrier E arising from the nanostructure:

$$D = D_0 \exp[-E/k_B T] \quad (1)$$

The case of diffusion along an interface is interesting, as it is highly sensitive to the degree of entanglement. In the unentangled, Rouse regime, chains can move along the interface without additional intermixing of blocks, and there is no new barrier. This situation is analogous to lipids moving along a bilayer. On the other hand, a well-entangled diblock will diffuse by reptation, which requires that one block enter the other domain to a significant extent, leading to a barrier proportional to $\chi N/N_e$, where N_e is the entanglement degree of polymerization. This picture was confirmed by extensive forced Rayleigh scattering (FRS) measurements of diffusion in well-aligned lamellae and cylinder phases.[57,58,60,61,63,67]

For D_{perp}, or for D in particles, the distinction between unentangled and entangled is primarily contained in D_0, and the experimental barrier is proportional to χN_{core}. This has been demonstrated in multiple systems; Figure 5 shows two particular examples. Cavicchi and co-workers used FRS forced

https://doi.org/10.1021/acspolymersau.2c00033
ACS Polym. Au 2022, 2, 397−416

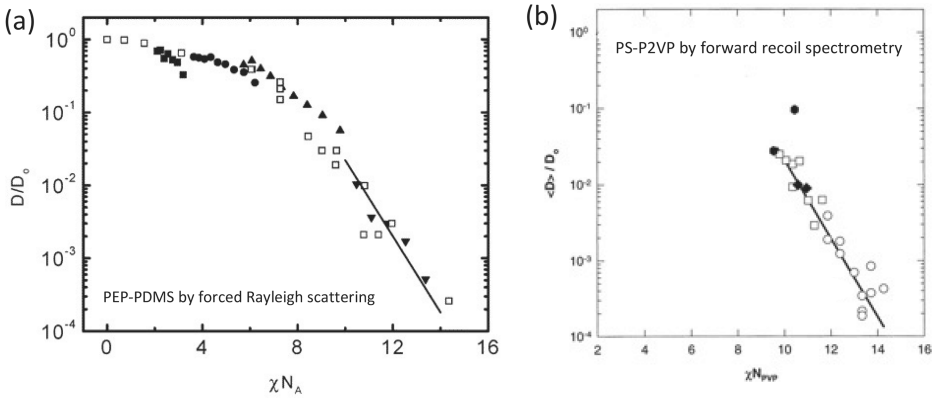

Figure 5. Tracer diffusion (D) of sphere-forming diblock copolymers in the melt, normalized to the diffusivity in the absence of structure (D_0), as a function of χ times the degree of polymerization of the core-forming block: (a) PEP−PDMS. Reproduced with permission from ref 66. Copyright 2003 American Chemical Society. (b) PS-P2VP. Reproduced with permission from ref 62. Copyright 1998 American Chemical Society. The straight line in each panel is the same, indicating the quantitative equivalence of the results.

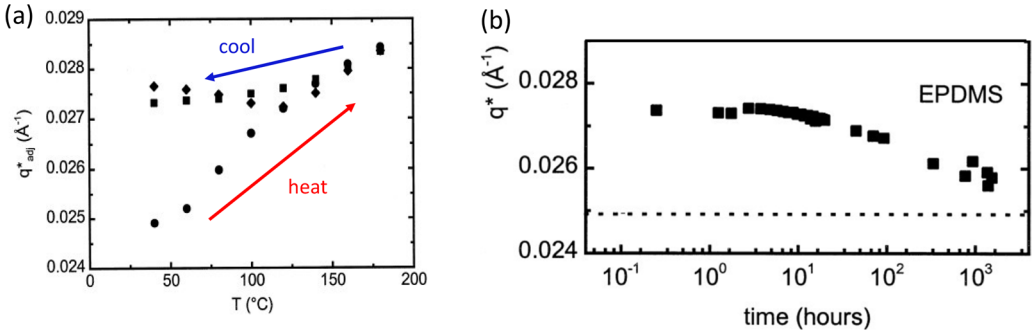

Figure 6. (a) Primary peak position q^* for PEP−PDMS diblocks in the BBC phase. The sample was annealed for many months at room temperature before the trace marked "heating". The sample was then cooled back (black squares) and departed from equilibrium below 150 °C. The sample in diamonds was quenched from 180 to 40 °C before heat. (b) Long-term annealing for q^* for the sample in panel a, after cooling to 40 °C. Reproduced with permission from ref 65. Copyright 2003 Wiley.

Rayleigh scattering (FRS) to follow diffusion of poly(ethylene-*alt*-propylene)-*b*-poly(dimethylsiloxane) (PEP−PDMS) in BCC-forming melts, with the results showing a clear crossover to $D/D_0 \sim \exp(-\chi N)$ with increasing N and with decreasing temperature (increasing χ), as shown in Figure 5a.[66] Yokoyama and Kramer used forward recoil spectrometry on polystyrene-*b*-poly(2-vinylpyridine) (PS-P2VP) diblocks in the BCC phase,[62] and the results between the two systems and the two techniques are quantitatively consistent (Figure 5b). The linear dependence of the barrier on N is not an obvious result. The theory of Halperin and Alexander assumes collapse of a core block into a globule on entering the "foreign domain", leading to a barrier varying as $N_{core}^{2/3}$.[40] Dormidontova's theory is also consistent with this result.[42] Interestingly, Helfand proposed an alternative mechanism for D_{perp} in a lamellar phase, whereby one block "hyperstretches" to traverse the other domain while exposing a minimal number of monomers at any time.[68] However, this model also leads to a barrier increasing with $N_{core}^{2/3}$.

Collectively, these results permit a reasonable estimate of the chain exchange time for any ordered array of spherical particles, using the sphere-to-sphere distance (e.g., from SAXS or SANS) and the diffusivity. The latter can be estimated from D_0 (which can be obtained from any measurement of D in the disordered state, and scaled appropriately with N and T) and the barrier. This chain exchange time sets a lower bound for how rapidly a sphere phase can adjust its mean aggregation number and domain spacing, upon changes in temperature. And, given that chain exchange alone cannot readily change the number density of micelles, this lower bound may still be orders of magnitude shorter than the equilibration time. An example of this phenomenon is provided in Figure 6.[65] Figure 6a shows the position of the primary peak (q^*) for a PEP−PDMS sample in the BCC phase. The sample was first annealed for many months, yielding a value for q^* below 0.025 Å^{-1} at 40 °C. The sample was then heated to 180 °C and q^* increased monotonically, consistent with the expected reduction in mean aggregation number Q and concomitant increase in micelle number density. The sample was then cooled back to 40 °C, and q^* (black squares) stopped decreasing near 120 °C. (The temperature dependence of q^* was corrected for changes in density, $\rho(T)$). The black diamonds correspond to a sample annealed at 180 °C, then quenched quickly to 40 °C, before heating. Clearly, the sample at 40 °C was far from equilibrium, even though it retained the BCC structure. The sample was then annealed at 40 °C for about three months, yielding the plot in Figure 6b. Even on this time scale, the sample did not achieve equilibrium (indicated by the dashed line). FRS measurements of D gave an exchange time of about 10 s at 140 °C and 1000 s at 40 °C,[66] values that are about 2−3 orders of magnitude shorter than the equilibration time implied by Figure 6b. Note that a lamellar sample of comparable molecular weight showed complete reversibility for $q^*(T)$

https://doi.org/10.1021/acspolymersau.2c00033
ACS Polym. Au 2022, 2, 397−416

over the same temperature range and that the glass transition temperatures of both blocks are well below 0 °C and, therefore, play no role. Note also that the phenomenon revealed by Figure 6 is a close analog to the solution data presented in Figure 3. These results also imply that, for any BCP system that is cooled from disorder into the BCC phase, the sample is unlikely to achieve equilibrium in terms of $Q(T)$ or $q^*(T)$, unless annealed for substantial amounts of time.

The process by which the BCC phase is able to equilibrate relatively rapidly upon heating is not entirely clear. Ejection of individual chains from micelles is relatively rapid, and has the additional benefit of lowering the free energy of the remaining micelle. The increase in free chain population could then favor nucleation of new micelles. On the other hand, individual spheres could also undergo "asymmetric" fragmentation, ejecting small clusters of chains that could serve as nuclei for new micelles, while leaving behind a micelle that is closer to the equilibrium aggregation number.

A fascinating recent development in melt block polymer self-assembly has been the discovery of Frank–Kasper (FK) phases, in which diblocks self-assemble into micelles of multiple distinct sizes, before packing onto a more elaborate lattice than BCC (see Figure 1).[10,69−73] For example, the sigma (σ), A15, C14, and C15 phases involve unit cells containing x spheres of y distinct sizes, where x = 30, 8, 12, 24 and y = 5, 2, 3, 2, respectively. Often, these phases emerge on cooling from a BCC phase, with nominally equivalent micelles. Therefore, there must be a new dimension to the required equilibration processes, involving redistribution of chains among micelles in addition to changes in total micelle number density. An example of this is shown in Figure 7, for the same low T_g

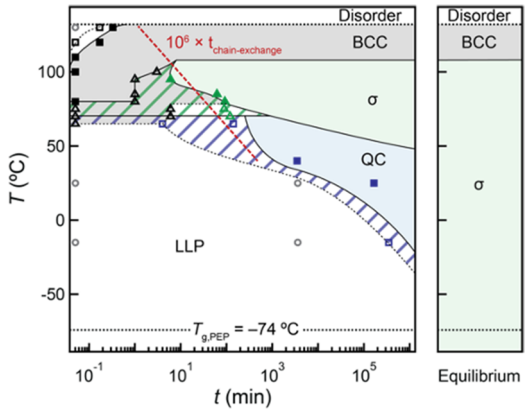

Figure 7. Time–temperature transformation diagram for a PEP–PDMS diblock subject to long-time annealing after various temperature quenches. The equilibrium phases are BCC and σ, but the latter takes increasingly long times to emerge at lower temperatures. This is attributed in part to slow dynamics; the red dashed line indicates the estimated chain exchange time. Reproduced with permission from ref 74. Copyright 2021 American Chemical Society.

system PEP–PDMS studied by forced Rayleigh scattering.[74] In this case, the sample undergoes an order–disorder transition from BCC near 130 °C, and an order–order transition into the σ phase near 105 °C. However, the σ phase can take many months to grow in, depending on annealing temperature. In the indicated time–temperature–transformation diagram, it is possible to supercool the BCC phase, and then the system develops a liquid-like packing (LLP) without a clear lattice symmetry. Upon annealing, a dodecagonal quasicrystal phase appears as a metastable intermediate on the path to σ. Also shown on the diagram is a dashed line indicating the temperature-dependent chain exchange time, but multiplied by a factor of 10^6. The similarity in slope is very suggestive that the barrier to equilibration tracks chain exchange but on much longer time scales. Furthermore, the large discrepancy between the time scales for chain exchange and full equilibration echoes the results in Figure 6. In any case, the emergence of FK phases and the associated prevalence of metastability underscores the need for more careful study of relaxation mechanisms in these systems.

IV. CHAIN EXCHANGE IN SOLUTION

IV.A. Surfactants

The theoretical model of Aniansson and Wall[33,34] predicts the rate of the fast relaxation process k_1 to increase linearly with the total surfactant concentration well above CMC, which is one key relationship that tests the validity of the theory. The consistency of the fast relaxation time τ_1 associated with insertion/expulsion of a single surfactant molecule to/from micelles with the experimental observations[35,44,75] is generally satisfactory for both ionic and nonionic surfactants, even though the theoretical model treats amphiphilic molecules as nonionic. However, the rate of the slow process k_2 is predicted to initially increase with total surfactant concentration, reaching a peak value slightly above the CMC, followed by a decrease with concentration well above the CMC. This nonmonotonic dependence of the rate of slow process on concentration is only in qualitative agreement with the experimental results.[35,44] In particular, the decrease in k_2 with concentration is found to be much steeper in experiments than predicted by the model, for most ionic systems investigated. Since the model has been developed for nonionic surfactants whereas the experimental systems involve ionic surfactants, the discrepancy has been attributed to the influence of electric charges of the headgroup and counterions. However, even for nonionic surfactants, such as Triton-X-100, the experimental results for k_2 are inconsistent with the theoretical predictions at high surfactant concentrations.[44] Lessner et al.[76] treated ionic micelles as charged colloidal particles interacting by DLVO forces. This model predicts a steeper decrease in k_2 with concentration, consistent with experiments. This theoretical analysis is in good agreement with experiments with ionic surfactants at both low and high counterion concentrations. Using the colloidal particle treatment of micelles as proposed by Lessner et al.,[76] Kahlweit has quantified the theoretical model and summarized the comparison of its predictions with the experimental results.[77] Overall, he concluded that for the ionic surfactants, the slow process occurs primarily by stepwise association and dissociation route at low ionic strength and by fusion and fragmentation mechanisms at sufficiently high ionic strength. For nonionic surfactants, the slow process is dominated by fusion and fragmentation mechanisms.

Several techniques have been utilized to study surfactant micelle relaxation behavior, such as temperature-jump, pressure-jump, shock tube, stopped-flow, synchrotron small-angle X-ray scattering, light absorption, fluorescence, solute exchange, and conductivity measurements.[35,75,78,48,79] In order to gain an understanding of the kinetics of micellization, the evolution of micelle shape and size during equilibration has been investigated in real-time using SAXS in combination with

https://doi.org/10.1021/acspolymersau.2c00033
ACS Polym. Au 2022, 2, 397–416

the stopped-flow mixing technique (see Figure 3).[48] The exchange of surfactant molecules between two types of micelles occurs at the time scale of 0.01−0.1 s resulting in mixed micelles. These spherically shaped mixed micelles are unstable and, therefore, undergo a fusion process to equilibrate toward cylindrical-shaped mixed micelles on the time scale of 0.1−1 s.[80] The ultrasonic relaxation method was used to investigate the kinetics of the exchange of surfactants between micelles and the bulk phase.[79] These results were also consistent with the theory of Aniansson and Wall.[33,34]

As noted in section II, surfactant exchange is a fast process. The bare relaxation time for a surfactant molecule in water (e.g., estimated from the Stokes−Einstein−Debye equation) is typically below 1 ns. A barrier on the order of 11 k_BT, say for a 10-carbon tail, would give an exchange time on the submillisecond time scale; even a 20-carbon tail, where equilibration is known to be more delicate, should still exchange on the order of seconds. Such rapid processes have been quantified by a variety of clever experimental techniques, particularly by taking advantage of a stopped-flow apparatus. Of particular relevance to this Perspective, the linearity of the exchange time on carbon number m has been well-established. Examples for several systems, couched in terms of the average residence time of a single surfactant in a micelle, are shown in Figure 8.

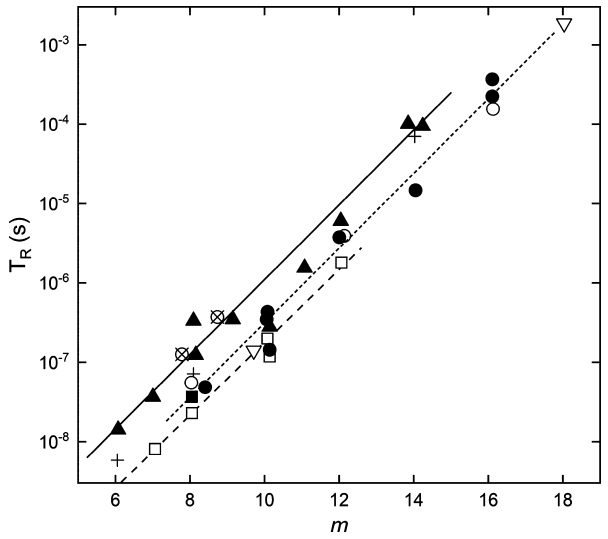

Figure 8. Residence time of individual surfactants in micelles for a variety of systems, as a function of carbon number m. Figure reconstructed from Figure 3.8 in ref 30.

Atomistic molecular dynamic simulations were performed to study the aggregation behavior of two types of surfactants—short-chained and comparatively long-chained surfactants. Short cationic surfactants comparatively showed faster monomer exchange.[81] A phenomenological free energy-based approach was proposed to model the kinetics of surfactant micellization.[82] This approach provides a more unified description of the kinetics rather than considering different stages as separate processes. Several relaxation processes, such as nucleation, growth, and final stage are captured as pathways on a single free-energy landscape. The growth of nuclei occurs at fast time scales, around 10^{-6}−10^{-5} s, which are similar to the fast relaxation time for the single monomer exchange process in classic models.

IV.B. Block Copolymer Exchange

The theory presented by Halperin and Alexander is the most thorough treatment of chain exchange in BCP micelles.[40,41] They also considered fragmentation and fusion but concluded that these processes would be much slower than exchange for a micelle close to, or at, equilibrium. For chain exchange, escape from the micelle core is assumed to be rate-limiting, with the key assumption that the core block collapses into a globule as it enters the corona, in order to shield unfavorable contacts with the surroundings. They then applied Kramers' rate theory to consider the trajectory of the core globule across the corona. Their key result is that

$$\tau_{esc} \sim \exp(\gamma a^2 N_{core}^{2/3}/k_BT) \quad (2)$$

where γ is the interfacial tension and a is the monomer size. The dependence of the barrier on $N_{core}^{2/3}$ is a direct consequence of the assumption of a collapsed globule. The unspecified prefactor in eq 2 incorporates a dependence on the corona block length (scaling as $N_{corona}^{9/5}$) for "star-like" micelles ($N_{corona} > N_{core}$), which is the more typical experimental situation.

Prior to the advent of time-resolved SANS, time-resolved and steady-state fluorescence measurements were used to study chain exchange rates (these techniques are described in Wang et al.[83]). In 1991, Cao et al.[84] used fluorescence probes clustered around the core−corona interface of the micelle in a PMMA-*b*-PS-*b*-PMMA triblock system and found that the rate-limiting step for molecular exchange was escape of the core block out of the micelle, confirming the assumption by Halperin and Alexander. Subsequent fluorescent experiments by Smith and Liu allowed them to formulate a model to describe the chain insertion process.[85] Wang et al. proceeded to measure an activation energy for chain exchange on the order of 10^2 kJ/mol for a polystyrene-*b*-poly(oxyethylene) system, slightly smaller than (but on the same order of magnitude as) the activation barrier for fragmentation.[86] Using nonradiative energy transfer, Prochazka et al. determined that the chain exchange rate was several orders of magnitude lower when the micelles were close to equilibrium, compared to systems with larger perturbations from equilibrium.[87] They attributed this effect to impaired chain mobility in the micelle core. Work by Creutz and co-workers[88] in diblock and triblock copolymer systems found that the exchange of chains between BCP aggregates is 10^9−10^{11} times slower than in surfactant systems and that by changing the hydrophilic/hydrophobic balance of the copolymers they could tune the chain exchange rate by a factor of 20.[89] Several groups followed up on this work by conducting studies of factors that tune the chain exchange rate. Underhill et al. determined for a polystyrene-*b*-poly(2-cinnamoylethyl methacrylate) in THF/cyclopentane system that increasing the corona block length led to an increase in the chain exchange rate.[90] They also studied the system-specific effects of changing N_{corona}/f_{core}, temperature, and solvent content. Rager et al., using poly(acrylic acid)-*b*-poly(methyl methacrylate) BCPs in mixtures of water/organic solvents, determined that changing the solvent to be chemically similar to the corona block did not affect the chain exchange rate but made the aggregation number Q smaller.[91] Further, van Stam et al. conducted a comprehensive study using a poly(styrene-*b*-sodium methacrylate) and poly(*tert*-butylstyrene-*b*-sodium methacrylate) systems in aqueous solution. They lowered the chain exchange rate

https://doi.org/10.1021/acspolymersau.2c00033
ACS Polym. Au 2022, 2, 397−416

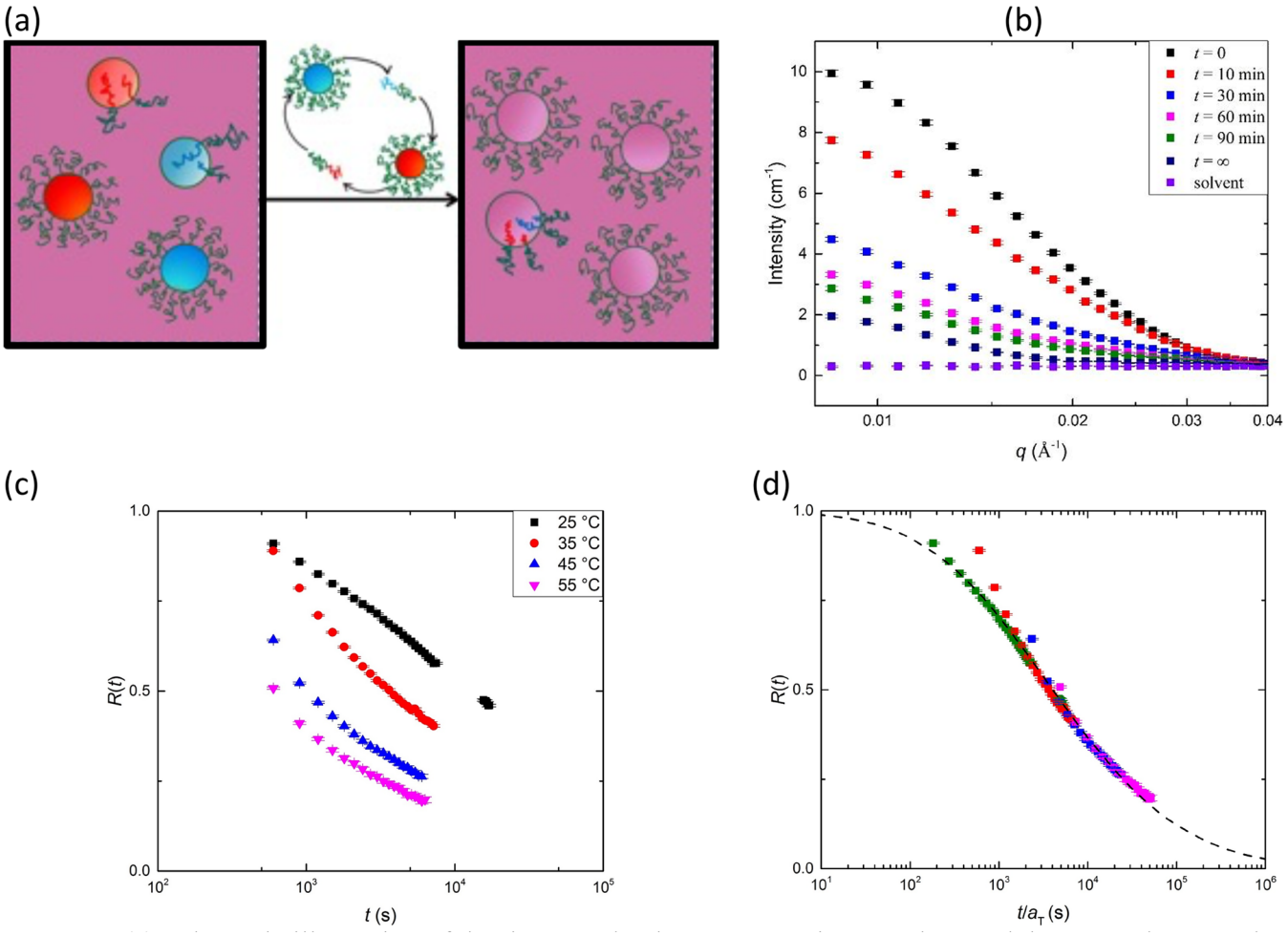

Figure 9. (a) Schematic illustration of the time-resolved SANS experiment, where red denotes a deuterated core block, blue a normal core block, and purple a solvent containing sufficient deuterium to contrast-match a 50:50 deuterated:normal core. (b) SANS traces as a function of time, after blending two micelle populations (in this case, PMMA-*b*-PnBMA in [C_2mim][TFSI]). Note that the infinite time data correspond to a sample in which the deuterated and normal BCPs were blended in advance. The fact that this SANS trace does not match the solvent is due to residual scattering from the PMMA coronas. (c) Relaxation functions $R(t)$ for equivalent blended samples at different temperatures. (d) Master curve obtained by horizontal shifting of the data in panel c with T_{ref} = 35 °C. The dashed curve is a fit to the model described by eq 4. Data reproduced with permission from ref 95. Copyright 2016 American Chemical Society.

using various methods: reducing the temperature, increasing N_{core}, and adding an unfavorable cosolvent.[92] Additionally, they use cosurfactants to perturb core/corona interfaces of the micelles.[92]

IV.C. Time-Resolved Small-Angle Neutron Scattering

There is no question that the advent of TR-SANS brought a uniquely powerful and quantitative means to examine chain exchange processes.[93,94] The basic approach is illustrated in Figure 9a. Two equivalent micelle populations are prepared: one with a "normal" core block and one that is deuterium-substituted to some extent (typically perdeuterated). The selected solvent is also an isotopic mixture with zero-average-contrast, meaning that the scattering length density of the solvent is exactly halfway between that of the normal and labeled cores. The two micelle populations are then mixed, forming a "post-mixed" sample, which exhibits significant scattering from both micelles. The sample is then annealed at a target temperature; as the exchange process randomizes the labeled chains, the intensity decays monotonically to zero. If the micelle size and shape remain approximately constant throughout the process, the functional form of the coherent intensity I with respect to the wavevector q remains constant; all that changes is the contrast factor. This is illustrated in Figure 9b for poly(methyl methacrylate)-*b*-poly(*n*-butyl methacrylate) (PnBMA-PMMA) diblocks in an ionic liquid.[95] A normalized relaxation function, $R(t)$, is obtained as

$$R(t) = \sqrt{\frac{I(q,t) - I(q,\infty)}{I(q,0) - I(q,\infty)}} = \sqrt{\frac{I(t) - I(\infty)}{I(0) - I(\infty)}} \quad (3)$$

where the initial intensity $I(0)$ corresponds to the postmixed sample and $I(\infty)$ reflects the fully equilibrated mixture.[96] As a check, the latter can be obtained from a "pre-mixed" sample, where the micelles are initially prepared from a 50:50 blend of normal and deuterated samples (shown as "$t = \infty$" in Figure 9b).

Measurements of $R(t)$ are performed at selected temperatures where the exchange is significant on the SANS time scale (typically 1−200 min; longer times can be accessed by annealing outside the beam). An example is shown in Figure 9c, for the same system; note the logarithmic time axis. With increasing temperature the relaxation is more rapid, as one might expect. However, this is an LCMT system, so increasing

https://doi.org/10.1021/acspolymersau.2c00033
ACS Polym. Au 2022, 2, 397−416

temperature accelerates dynamics but also increases the barrier, due to the increase in χ; the effect on dynamics is greater. The curves obtained at different temperatures can then be shifted horizontally to obtain a master curve, by time−temperature superposition (tTs); the result in this case is shown in Figure 9d. The use of tTs is just as useful as it is in rheology, potentially extending the dynamic range of TR-SANS to over 12 decades.[97] This occurs in systems, such as polystyrene-*b*-poly(ethylene-*alt*-propylene) (PS-PEP) with PS cores, where the glass transition of the PS controls the segmental dynamics of an escaping chain.

In contrast to the prediction of the Halperin−Alexander theory but in agreement with the melt self-diffusion results discussed in section III, the barrier to chain exchange is found to increase linearly with N_{core}. An example is shown in Figure 10, for PS-PEP in squalane.[98] Two values of N_{core} were used,

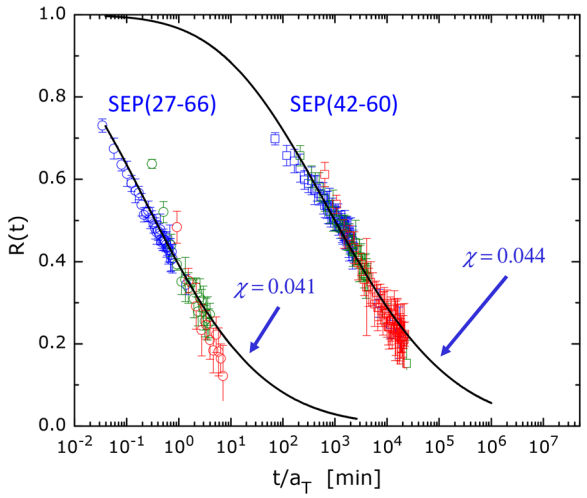

Figure 10. TR-SANS relaxation function for two PS-PEP samples, with fits to eq 4. The extracted value of χ is independent of N if the barrier is taken as increasing linearly with N_{core}. Figure reconstructed from data in ref 98.

which only differed by a factor of about 1.5; the larger polymer exchanged almost 4 orders of magnitude more slowly. Both $R(t)$ curves were described by the model summarized below, with a consistent value of an apparent $\chi \approx 0.04$ and a core block dispersity $Đ \approx 1.08$. A similar conclusion with respect to the N_{core} dependence was reached by Zinn et al.[99] and by Ma et al.[95] The model proposed by Choi et al.[98] invoked a convolution of a single exponential decay for a monodisperse polymer with the chain length distribution of the core block, as shown in the equation

$$R(t) = \int_0^\infty P(N_{core})\exp\left(-\frac{t}{\tau_{esc}}\right)dN_{core} = \int_0^\infty P(N_{core})\exp(-\{t/\tau_{core}\exp[f(\chi)N_{core}]\})dN_{core} \quad (4)$$

where the time constant for the decay τ_{esc} includes the barrier, and thus, the overall function represents an exponential of an exponential in N_{core}, yielding the hypersensitivity to dispersity observed in Figure 10 (note the logarithmic time axis). Zinn et al. provided a direct confirmation of this interpretation; a monodisperse core block yields a single exponential decay for $R(t)$, in this case for an alkane(C_{24})-PEO copolymer in water.[99] In eq 4, the barrier is written as $f(\chi)N_{core}$, although this is often simplified to χN_{core}. One possible explanation for the linear dependence of the barrier to exchange with respect to N_{core} will be discussed subsequently.

The dependence of the exchange rate on corona block length is also interesting. The theory of Alexander and Halperin predicts that an increase in corona length will *retard* exchange, as the collapsed core block is presented with a wider foreign domain to traverse. Measurements by Zinn et al., on alkane-PEO diblocks in water are consistent with this expectation (see Figure 11a).[100] On the other hand, early fluorescence measurements by Underhill et al. led to the opposite conclusion.[90] More recently, TR-SANS measurements by Wang et al. also showed an *acceleration* of exchange in PS-PEP micelles with longer PEP coronas (Figure 11b).[101] Both groups attributed this result to the relief of corona chain stretching upon escaping a micelle, which would lower the net barrier to expulsion relative to the contribution from the core block.

The dependence of the barrier on the strength of the interaction between the core block and the surrounding medium is likely more complicated than in the melt case discussed in section III; in other words, $f(\chi)$ in eq 4 is not simply equal to χ. Presumably the barrier increases with the core−solvent interaction, embodied in the Flory−Huggins

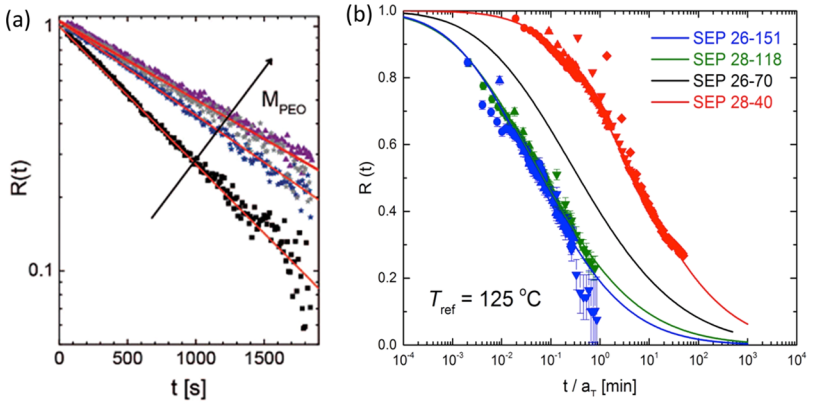

Figure 11. Effect of N_{corona} on chain exchange: (a) C_{24}−PEO in water and (b) PS-PEP in squalene. The two systems show opposite trends. Figures reproduced with permission from ref 100, copyright 2016 American Chemical Society, and ref 101, copyright 2018 American Chemical Society, respectively.

https://doi.org/10.1021/acspolymersau.2c00033
ACS Polym. Au 2022, 2, 397−416

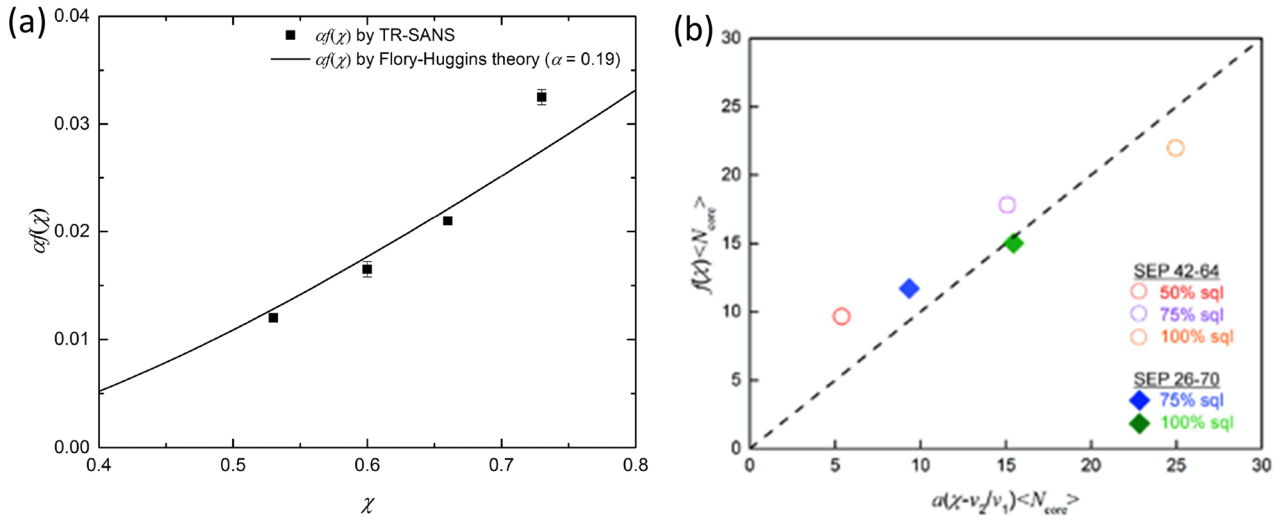

Figure 12. (a) Dependence of barrier divided by N_{core}, $\alpha f(\chi)$, on the independently determined χ, for PnBMA-PMMA in $[C_2mim][TFSI]$. (b) Enthalpy penalty of chain expulsion for SEP micelles in binary mixed solvents, comparing the fitted results from TR-SANS ($f(\chi)\langle N_{core}\rangle$) and calculated values by the Flory–Huggins theory ($a(\chi - \nu 2/\nu 1)\ \langle N_{core}\rangle$. Figures reproduced with permission from ref 95, copyright 2016 American Chemical Society, and ref 102, copyright 2020 American Chemical Society, respectively.

interaction parameter $\chi_{core\text{-}sol}$, or equivalently with the corresponding interfacial tension γ. However, the quantitative details are more complicated because, in order for micelles to form, it is necessary that $\chi_{core\text{-}sol} > 0.5$. Therefore, there must be an offset, such that the barrier becomes very small as the critical micelle temperature is approached. This idea has been explored in two studies, illustrated in Figures 12a and 12b, corresponding to PnBMA-PMMA in $[C_2mim][TFSI]$ and PS-PEP in mixtures of squalene and phenyldodecane, respectively.[95,102] In both cases an approximate attempt is made to relate the observed barrier to an independently determined $\chi_{core\text{-}sol}$, with some promise. However, this is definitely an area where more theory could be useful.

The preceding discussion has emphasized the dependence of chain exchange on intrinsic molecular variables (N_{core}, N_{corona}, χ). However, extrinsic factors can also play a role, including micelle concentration, aggregation number, and shape. In the dilute micelle regime, TR-SANS measurements on several systems have confirmed no dependence for τ_{esc} on concentration, consistent with the standard assumptions that (a) chain expulsion is the rate-limiting step and (b) fusion/fragmentation processes play a very minor role. One study extended the measurements into the more concentrated regime, where the PS-PEP micelles adopted a BCC macrolattice.[103] The results indicated a significant slowing down of exchange, which was attributed to the overlap of the corona chains removing any entropic benefit to liberating a corona block from a micelle. This conclusion was supported by separate measurements in which free PEP chains were added to an otherwise dilute micellar solution and which yielded a comparable slowing down of exchange.[104] Nevertheless, more extensive measurements of the concentration dependence of exchange, even all the way to the melt, would be welcome. This is challenging to accomplish with TR-SANS, due to difficulties in preparing random mixtures of labeled and unlabeled micelles on ordered lattices. Self-diffusion measurements, for example by forced Rayleigh scattering, could be one promising route.

Measurements by Zhao et al. indicate that chain exchange also depends on the micelle size.[105] By using two different preparation routes, direct dissolution and cosolvent evaporation, as described above, the authors created micelles of two distinct sizes from the same diblocks. They further confirmed that the micelle size did not change over the time scale of the TR-SANS measurements. The exchange time was a factor of 3 larger for the larger micelles, an effect that was tentatively attributed to the denser corona in the larger micelles.

There have been almost no measurements of chain exchange in nonspherical block polymer aggregates (e.g., vesicles or wormlike micelles), although a great deal is known about dynamics of lipid vesicles. A pioneering study by Lund et al. found that exchange was slightly faster for a given PEP-PEO copolymer in spherical micelles compared to worm-like micelles, although it should be noted that the sphere-to-cylinder transition was effected by increasing χ.[106] Further TR-SANS measurements for given BCPs in different micellar structures would certainly be warranted.

Chain architecture can play a huge role, as illustrated in studies of chain exchange in PEP-PS-PEP versus PS-PEP-PS triblocks.[107] In the former case, the PS core block was kept constant, and a second PEP block was added to the chain. The resulting micelles were, as expected, significantly smaller than for a matched diblock with the same PS and PEP block molecular weights. Similarly, the triblocks underwent chain exchange more than 3 orders of magnitude more rapidly than the diblocks, an effect that surely transcends the role of core size. This result also indicates that, while the penalty for placing the core block into the solvent is still the major contributor to the barrier, it is far from the only important factor. The PS-PEP-PS triblocks, on the other hand, formed predominantly "flower-like" micelles at low concentrations.[108] The rate of exchange was much slower than a diblock with the same PS block, and a full 10 orders of magnitude slower than the inverse polymer. The fact that these measurements could be accomplished underscores the power of time–temperature superposition in this context. Yokoyama et al. had previously considered the diffusion of triblocks in BCC melts, and proposed a "chain walking" mechanism, whereby each end-block pulls out independently, and inserts into a neighboring micelle.[64] Based on the diblock exchange, Lu et al. could

https://doi.org/10.1021/acspolymersau.2c00033
ACS Polym. Au 2022, 2, 397–416

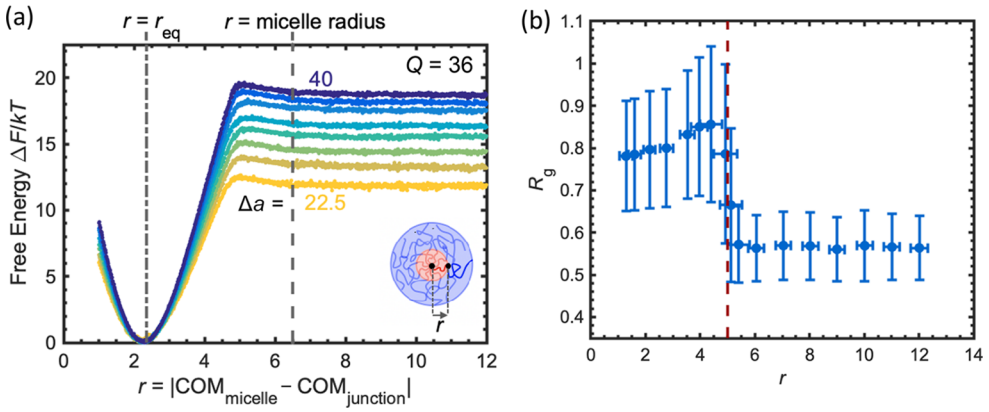

Figure 13. (a) Free energy of a single A_4B_8 BCP as a function of the distance between the block junction and the micelle center-of-mass, as a function of the core−solvent energy. Data reported in ref 114, corrected for the entropy of the spherical shell.[124] (b) Stretching of the core block as a function of position. Figure reproduced with permission from ref 114. Copyright 2021 American Chemical Society.

estimate the rate of triblock exchange;[107] the comparison indicates that there is a slightly enhanced probability for the second core block to escape once the first block has succeeded. Another interesting aspect of the PS-PEP-PS case is its relation to the dynamics of physical gels formed by thermoplastic elastomers. In this case, surprisingly, the pull-out time implied by TR-SANS is much longer than the stress−relaxation time measured on PS-PEP-PS gels by rheological means. This apparent discrepancy has been explored in some detail by Peters.[109] The Choi group has also recently initiated an interesting new direction, the study of chain exchange in bottlebrush BCPs.[110]

IV.D. Simulations of Chain Exchange

Coarse-grained polymer simulations have played an important role in understanding chain exchange between micelles. Dissipative particle dynamics[111] (DPD) is the most common methodology, following the pioneering work by Li and Dormidontova applying DPD to micellization kinetics.[112] The key advantages of DPD relative to other dynamical simulation methods[112] are that (i) DPD correctly incorporates hydrodynamic interactions through an explicit solvent, which are likely relevant for distinguishing between Rouse diffusion of the hydrophobic block when it is inside the micelle core and Zimm diffusion of the chain when it is released into the solvent,[113] and (ii) DPD uses relatively soft interaction potentials, which permit large time steps[111] that can access the time scales relevant for unimer exchange that would be infeasible using the potentials required for atomistically detailed simulations. Even with a soft potential, however, rather high degrees of coarse graining are needed to simulate micelle dynamics. For example, multiple DPD simulations[112−115] use two or four DPD beads to represent the hydrophobic block. If this model is intended to describe a typical experiment (e.g., polystyrene with 250 or 400 repeat units[98]), each bead represents *ca.* 100 repeat units.

The most common application of DPD simulations directly mimics the TR-SANS experiment, artificially "labeling" chains in the simulation as deuterated and then computing the contrast relaxation from the coordinates of those labeled chains. Such TR-SANS simulations have been performed for AB diblock copolymers,[113,115,116] linear BAB triblock copolymers with solvophobic middle blocks[116,117] and the corresponding branched AB_1B_2 triblock copolymers,[117] mixtures of linear diblocks, and tadpole diblocks with circular solvophobic blocks,[118] and tadpole diblocks with circular solvophilic blocks.[119] An especially notable outcome of these simulations was the observation[3] of a single exponential decay with an exponent that is linear in the solvophobic block length, consistent with experimental data and in contrast to the predictions of the scaling theory of Halperin and Alexander.[40] However, one should view this conclusion as potentially arising from a limitation of the DPD model and the small (N_A = 4) core block size; much larger N would be necessary to create the dry, collapsed globule in the Halperin and Alexander theory.[120] Such large-scale simulations that further capture micellization are feasible but expensive;[121] the lower bound for DPD simulations of the coil−globule transition corresponded to at least 80 beads, substantially larger than any core block used for micelle exchange.[120] The presence of artifacts due to the small discretization, especially in connection to solvophobic-block collapse, is suggested by the escape of small aggregates in these DPD simulations,[113] which could be shielding the solvophobic blocks in manner that is not captured by a very coarse-grained model that cannot provide globular collapse of a single block.

In addition to directly simulating an experimental observable, such as the relaxation in TR-SANS, simulations are powerful for probing features that cannot be readily observed in experiments. A natural starting point is interrogating chain conformations during the escape process, for example how the configurations of escaping BAB triblocks, which form looped solvophobic blocks that simultaneously pull out of the micelle core, differ from their AB diblock counterparts, which escape bead-by-bead.[117] An even more powerful application is to directly measure the free energy barrier for unimer escape[114] through a combination of umbrella sampling[122] and a weighted-histogram analysis method (WHAM),[123] following analogous work for small molecule surfactants.[124] In this approach, a stiff biasing potential is applied to the junction point in an AB diblock polymer to constrain its location near a fixed distance relative to the micelle core. Combining simulation data obtained for many such fixed distances with WHAM provides a measure of the full free energy landscape for chain escape. As seen in Figure 13a, the biasing in the simulations allows access to very large free energy barriers, *ca.* 10−20 k_BT, that are comparable to those extracted from TR-SANS measurements,[98] that is, one can thus probe the experimentally relevant limit where chain exchange is slow

https://doi.org/10.1021/acspolymersau.2c00033
ACS Polym. Au 2022, 2, 397−416

compared to the segmental diffusion time. In addition to demonstrating that the free energy barrier is linear in the AB interaction energy, these simulations also provide information about the conformation of polymer chains at the transition state, which is neither fully stretched nor collapsed (Figure 13b).[114] Intriguingly, upon first departing the core, the core block stretches, and only collapses once it is past the transition state. This is in direct contrast to the globule assumption, and offers a potential explanation for the linear dependence of the exchange barrier on N_{core}. However, as a cautionary note, the extremely coarse-grained nature of the DPD approach may not be suitable to assess conformations of real polymers; as noted above, a 4-bead block cannot really adopt a globular conformation. Umbrella sampling methods have also been deployed to understand the relative rates of single chain exchange and micelle fusion and fission, leveraging a semigrand ensemble to identify both the most probable aggregation number and the kinetic rates for chain exchange. The latter work is an outstanding example of the power of biased sampling methods for micelle dynamics, probing seven orders-of-magnitude in rate constants.[125−127]

In addition to DPD simulations, Mackie and co-workers have used a dynamical single-chain in mean-field (SCMF) simulations to model the dynamics of chain exchange in an array of micelles formed by triblock copolymers, again mimicking the TR-SANS experiment.[128−130] A remarkable outcome of their calculations is the presence of a logarithmic decay despite their simulations using a monodisperse polymer.[129] They argue that the logarithmic behavior emerges from a degeneracy in the states available to the solvophobic midblock in the micelle core that is destroyed when that block escapes from the micelle core. The escape of the triblock polymer from the micelle in these SCMF simulations involves a subtle change in the radius of gyration that corresponds to neither complete stretching nor globular collapse,[128] similar to observations of the transition state in umbrella sampling of the escape of a diblock copolymer from a micelle.[114]

V. FRAGMENTATION/FUSION IN SOLUTION

V.A. Surfactants and Lipids

Fusion and fragmentation processes in lipid membranes and surfactant micelles have been extensively studied, in part because they are considered essential processes in a spectrum of pivotal biological/chemical functions.[131−133] Several methods have been used to monitor these processes in equilibrium surfactant micelles; stopped-flow fluorescence, pressure-jump (p-jump), temperature-jump (T-jump), SAXS, dynamic light scattering (DLS), and ultrasonic relaxation time-scan measurements. Of these the use of fluorescence-based techniques is most notable. For example, if micelles are prepared that contain either an insoluble donor or an insoluble acceptor, the growth of donor−acceptor fluorescence with time requires fusion to have taken place; the rate should be second-order with respect to micelle concentration. Similarly, if one begins with some micelles containing more than two excimer-forming fluorophores on average, mixing with identical empty micelles will lead to a drop in excimer fluorescence due to fragmentation. This process, in contrast, should be first-order in micelle concentration. In both cases, a constant average micelle size guarantees that the rates of fusion and fragmentation are balanced.

Since fusion and fragmentation are expected to be relatively slow, they are often triggered by introducing salts, surfactants, and ions, or by applying light or heat to perturb the system away from equilibrium. The pioneering work on fusion and fragmentation between two surfactant micelles were summarized by Zana.[134] Pyrene excimer formation in nonionic surfactant micelles followed second-order kinetics in micelle concentration, corresponding to fusion accompanied by fragmentation. Lowering the solubility of the solute in water by using triglyceride-substituted pyrene inhibits the direct exit/reentry of solutes into micelles, which otherwise competes with micelle fusion/fragmentation for solute exchange. Rharbi and co-workers examined exchange of the insoluble solute between nonionic surfactant micelles at high concentrations of surfactants,[37] at elevated temperatures,[135] or upon addition of salt.[136] In particular, they proposed that the increasing counterion concentration reduces electrostatic repulsions between adjacent headgroups, helping the headgroups to come into close contact, resulting in accelerated fragmentation. According to the proposed mechanism, a higher fraction of charged molecules in micelles slows both fusion and fragmentation.[37] However, the dominating mechanisms for fusion and fragmentation are still subjects of debate.[80,133] Fusion and fragmentation processes can also be directly visualized, as shown by Menger and Balachander with giant vesicles by light microscopy.[137] Vesicles with radii of 10−200 μm were made from a cationic amphiphile at 17 °C. Under high salt concentration, the giant vesicles eject smaller vesicles by a budding process, followed by fusion of two of small vesicles, which could be captured in the act of coupling.

Computer simulations of fusion and fragmentation were conducted by Pool and Bolhuis.[138] The formation of an interdigitating stalk prior to fragmentation was suggested by Sammalkorpi et al.,[139] and three intermediate stages for fusion were suggested by Li et al.:[140] (1) molecular contact, (2) formation of a neck between two micelles, and (3) growth of this neck, making one particle. Fragmentation was examined in detail by Gao et al.[141] More recently Ghosh et al. reported "solute-induced" budding and fragmentation processes of small lipid nanovesicles (<50 nm) by using coarse-grained MD simulations.[142] This simulation reveals a mechanism that reflects the interplay between membrane elasticity and solute-mediated membrane adhesion.

V.B. Block Copolymer Fusion and Fragmentation

As mentioned previously, Dormidontova presented a broad-ranging scaling analysis of the fusion and fragmentation processes for block copolymer micelles.[42] An example of the schematic reaction coordinate for fusion is provided in Figure 14. While the respective barrier height depends on the aggregation numbers of the merging micelles, Q_1 and Q_2, the time constants are very sensitive to the time scales of corona chain dynamics. Few of the resulting predictions have been subject to systematic experimental examination.

Rharbi and co-workers pioneered research into the fusion and fragmentation of polymeric micelles.[143] By using fluorescence decay methods, Rharbi showed that fusion and fragmentation occurred between micelles made by poly(ethylene oxide)-b-poly(propylene oxide)-b-poly(ethylene oxide) (PEO-PPO-PEO) at a rate about a factor of 10^6 slower than chain exchange, and also more than 10^6 times slower than surfactant micelles.[134] An example of this approach is shown in Figure 15, which illustrates how the measured decay of

https://doi.org/10.1021/acspolymersau.2c00033
ACS Polym. Au 2022, 2, 397−416

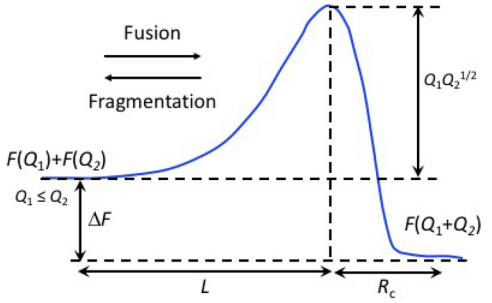

Figure 14. Schematic "reaction coordinate" for fusion/fragmentation, for micelles of sizes Q_1 and Q_2; fusion is favored in this case, as $\Delta F > 0$, following Dormidontova.[42] The barrier increases as $Q_1Q_2^{1/2}$; the time for one corona to penetrate the other to a distance L provides $\tau_{frag,0}$.

fluorescence as a function of empty micelle concentration yields a first-order rate constant, associated with fragmentation, and a second-order rate constant, assigned to fusion. In this more recent study, the authors particularly focused on the role of the PPO block length.[144] Somewhat surprisingly, the rates of fragmentation differed by up to 5 orders of magnitude for triblocks that do not differ greatly in molecular weight or composition. Furthermore, the apparent activation energies range from −80 to +100 kJ/mol, which is hard to reconcile with the expectation that these micelles follow the same mechanisms.

More recently, fusion events between small, nonequilibrated micelles of polybutadiene-*b*-poly(ethylene oxide) (PB-PEO) were monitored by Kelley et al.[145] Small polymeric micelles prepared by the cosolvent method grew through dialysis from the less selective THF into more selective water. A distinctly bimodal size distribution was taken as evidence for the micelle fusion process, as provided by a powerful combination of DLS, TEM, and SAXS measurements. They proposed the energy barrier to fuse two micelles as the steric repulsion or the elastic energy of the corona block. In a follow-up paper, it was clearly demonstrated that solution agitation and the accompanying air−water interface could markedly accelerate equilibration.[146] The fusion and fragmentation of polymeric micelles can also be directly imaged by microscopy. Polymer vesicles, especially branched-polymersomes generated from an amphiphilic multiarm copolymer (HBPO-*star*-PEO) in water, were the first example where the BCP fusion process was viewed by optical microscopy.[147] The entire fusion of two vesicles took about 1.5 min, which is much longer than the fusion time of liposomes (seconds) and biomembranes (milliseconds). More recently, liquid-cell transmission electron microscopy (TEM) enabled direct observation of the fusion of individual amphiphilic block copolymer micelles in solution.[148] These observations revealed growth and evolution occurring by both unimer addition processes and by particle−particle collision-and-fusion events. An intriguing example is shown in Figure 16, reproduced from Parent et al.[148]

Meli et al. pioneered a quantitative study of fragmentation in micelles prepared from PB-PEO copolymers in imidazolium-based ionic liquids (ILs).[149,150] By using the direct dissolution protocol, spherical micelles could be prepared that were significantly larger than the equilibrium size. The nonvolatility of the IL enabled prolonged annealing at elevated temperatures, and ultimately even direct imaging in liquid-phase TEM. The evolution of micelle size and size distribution was followed by a combination of DLS, SAXS, and TEM, all of which gave consistent results. An example of the use of synchrotron SAXS is given in Figure 17a; the spherical form factor of the core is clearly apparent, and the first minimum (indicative of R_{core}) evolves steadily over the course of 2 days.[151] The data can be described by a relaxation function which is a compressed exponential, defined by

$$R(t) = \frac{R_x(t) - R_x(\infty)}{R_x(0) - R_x(\infty)} = \exp(-[t/\tau]^n) \quad (5)$$

where R_x is the corresponding radius (i.e., R_{core} from SAXS, R_h from DLS) and n is an "Avrami" exponent. Often, it is found that $n \approx 2$, rather than the expected $n = 1$; the reasons for this functional form remain to be fully elucidated. An example is shown in Figure 17b, where the relaxation function is shown for a given polymer in five different ILs (with different γ).[152] In all cases, the data are well-described by eq 5 with $n \approx 2$. Furthermore, the time constants in the various solvents are not drastically different, suggesting that the fragmentation barrier does not involve exposure of the core to the solvent (which would presumably confer a sensitivity to γ, which varies by a factor of at least three over this sequence of solvents). The fragmentation rates are also independent of micelle concentration, as expected for a unimicellar process. The rates of fragmentation are strongly dependent on total molecular

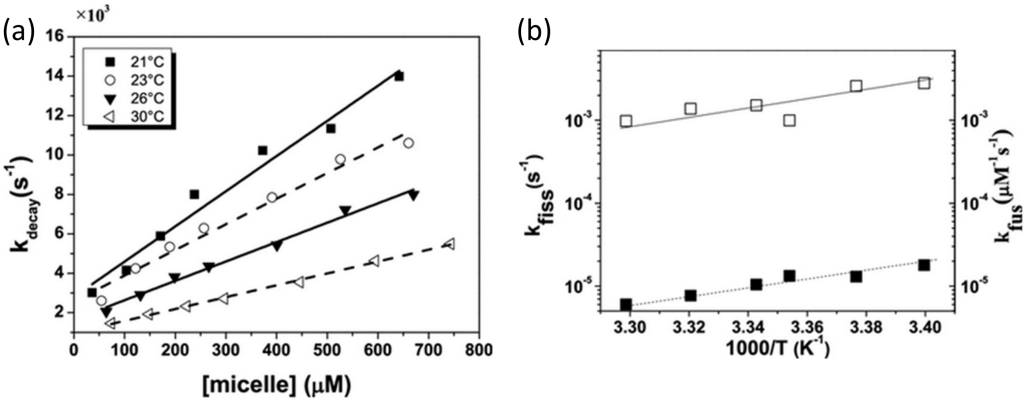

Figure 15. (a) Relaxation rates k_{decay} versus the concentration of P103 empty micelles for various temperatures: 21, 23, 26, and 30 °C. The concentration of micelles is given by ([micelles] = ([P103] − cmc)/N_{agg}. (b) Rate of fragmentation k_{frag} (□) and the rate of fusion k_{fus} (■) vs the inverse of the absolute temperature for P103. Figures reproduced with permission from ref 144. Copyright 2021 American Chemical Society.

https://doi.org/10.1021/acspolymersau.2c00033
ACS Polym. Au 2022, 2, 397−416

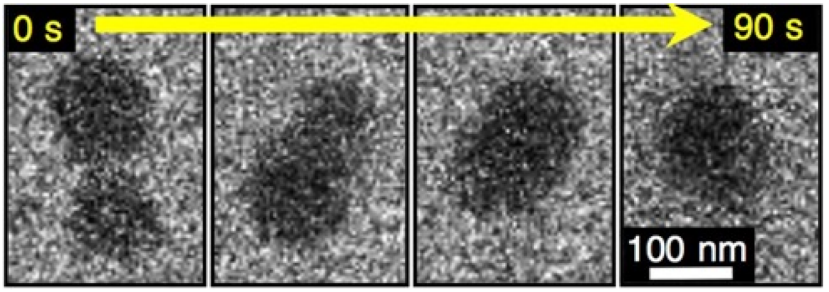

Figure 16. Liquid cell TEM images of a phenyl-*b*-peptide-*co*-hydroxyl amphiphilic BCP undergoing fusion in aqueous media. Reproduced with permission from ref 148. Copyright 2017 American Chemical Society.

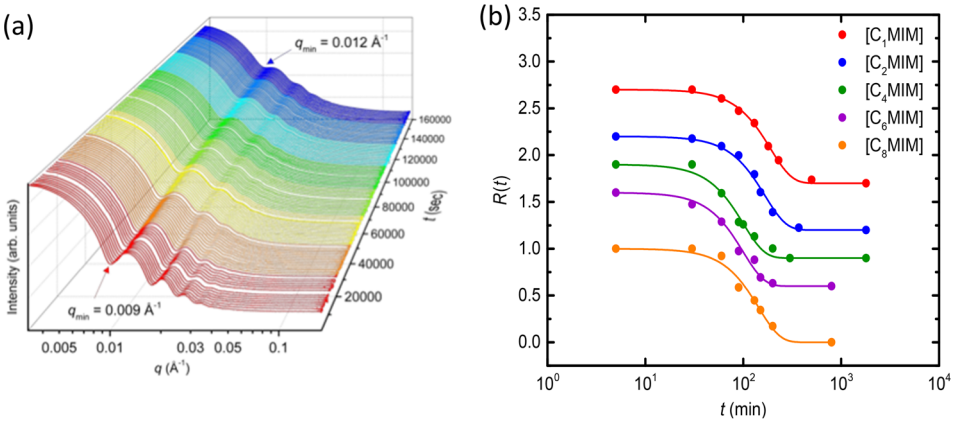

Figure 17. (a) Synchrotron SAXS for 0.25 wt % BO(25−22) in [C_2mim][TFSI] at 170 °C; (b) normalized $\langle R_{core} \rangle$ from SAXS upon T-jump to 170 °C for 0.5 wt % BO(8−7) in 1-alkyl-3-methylimidazolium [TFSI]-based ionic liquids. The curves are shifted vertically for clarity. Solid lines represent the fits to the relaxation function shown in eq 5 with an Avrami exponent of $n = 2$. Figures reproduced with permission from refs 151, copyright 2020 American Chemical Society, and 152, copyright 2019 American Chemical Society, respectively.

weight and independent of technique, as illustrated in Figure 18.[153] The observed power law exponent (9/5) is consistent with the Dormidontova theory, although strictly the prediction applies to N_{corona} rather than N_{total}.

As emphasized above, the negligible vapor pressure of ILs allows *in situ* liquid-phase TEM measurements. Examples of a time series for PB-PEO at 170 °C are shown in Figure 19.[151] The time indicates when the images were taken during annealing; actual exposure times are necessarily only a few seconds to avoid beam damage. Nevertheless, it is possible to capture transient structures, such as ellipsoidal micelles and "peanut-shaped" particles that are reminiscent of the anaphase state of a cell undergoing mitosis. A series of cartoons is provided to represent the process. These images are appealingly consistent with the earlier DPD simulations of Gao et al.[141]

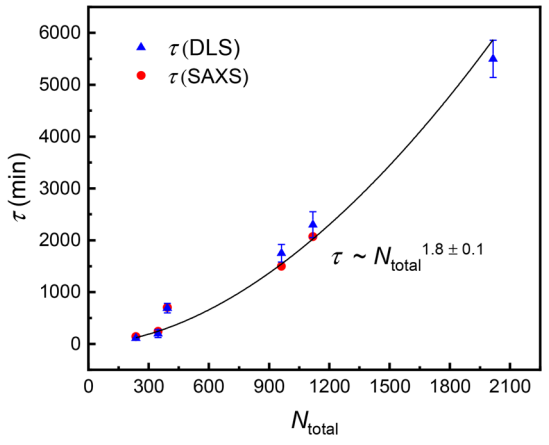

Figure 18. Fragmentation times for symmetric BO diblocks in [C_2mim][TFSI] as a function of total molecular weight, with the best fit power law. Reproduced with permission from ref 153. Copyright 2021 American Chemical Society.

An alternate route to insight about fusion and fragmentation mechanisms and rates is by monitoring the time-dependent transformation of one particle shape into another. Of particular interest are order−order transitions between BCC spheres and hexagonally packed cylinders in the bulk and shape transitions between worm-like and spherical micelles in solution. The former were anticipated by the pioneering theoretical work of Leibler[6] and have since been observed in multiple systems. One study in particular focused on the reversibility and heating/cooling rate dependence of the BCC⟨−⟩HEX transition in a PS-PI-PS triblock, which had an OOT at 196 °C.[154] The sample was shear-aligned in the HEX phase, which resulted in highly organized BCC phase above the OOT. The cylinder-to-sphere transition in this case proceeds through anisotropic fluctuations (with BCC symmetry) imposed on the cylinders. The hysteresis loop on successive heating and cooling cycles was monitored, and full reversibility was approached for rates below ±0.1 °C/min. TEM was used to examine intermediates during the cylinder-to-sphere transition, but not the inverse. Consequently, it was not possible to say whether the cylinders emerged by a uniaxial fusion of particles, or not. Nevertheless, this system apparently exhibits has the

https://doi.org/10.1021/acspolymersau.2c00033
ACS Polym. Au 2022, 2, 397−416

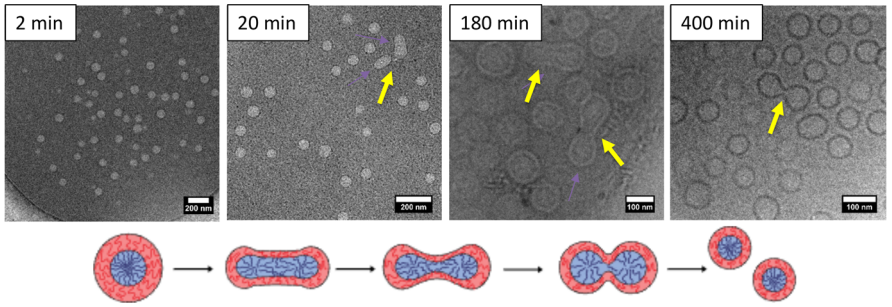

Figure 19. Time evolution of micelle cores for BO(25−22) in [C_2mim][TFSI] annealed at 170 °C directly in the TEM instrument.[151] Suggested pathway for fragmentation is shown below the images. Reproduced with permission from ref 151. Copyright 2020 American Chemical Society.

appropriate combination of time scales and temperature to allow more detailed examination of the mechanisms of OOTs.

A system that showed similarly thermoreversible micellar shape transitions in solution was reported by Abbas et al.[155] A PS-PDMS diblock dissolved in dialkyl phthalates showed vesicles, worm-like micelles, and spheres as a function of solvent composition, and as a function of temperature at a given composition. As the low-T_g PDMS block formed the micellar cores, chain motion was relatively facile, and the sphere-to-worm transition was thermally fully reversible on a time scale of minutes. Presumably the relatively short PS corona block ($M \approx 4$ kDa) enabled the rapid fusion of spherical micelles. In a similar vein, Landazuri et al. followed the kinetics of the sphere to worm transition in a PEO-PPO-PEO triblock solution subjected to temperature jumps.[156] The authors concluded that the dominant process was a random fusion-fragmentation process, akin to a step-growth polymerization, as opposed to a nucleation-and-growth process, akin to chain-growth. Cornel and co-workers took the approach of blending two populations of poly(lauryl methacrylate)-*b*-poly(methyl methacrylate) micelles and following the approach to an equilibrium population of hybrid micelles by SAXS.[157] They concluded that a combination of chain exchange and fusion/fragmentation were operative. Lund et al. followed the reverse process, of cylindrical micelles fragmenting into spheres, by both SAXS and SANS.[158] They found that the cylinders fragmented directly into spheres, but the resulting particles then coarsened to achieve the equilibrium Q.

These studies demonstrate the feasibility of studying fusion/fragmentation processes in detail through shape changes. It should be noted that in these examples the experiments were conducted relatively close to the corresponding ODT or CMT. One might expect, therefore, that contributions from chain exchange could be substantial and that it might be difficult to resolve the rates of "pure fusion" or "pure fragmentation" cleanly. However, this difficulty persists in almost all studies of these processes, so the promise of this approach is not diminished.

VI. SUMMARY AND OUTSTANDING ISSUES

In comparison to their low molar mass amphiphile analogs, BCPs are notoriously slow to adopt equilibrium nanostructures, in both solution and bulk. This is a direct consequence of large barriers to drag one block through a domain rich in the other, or through an unfavorable solvent. While high glass transition temperatures and high degrees of entanglement can retard equilibration even further, they are not required for a given system to be deeply metastable. Empirically, the rate of equilibration of particle phases and associated micelle aggregation numbers Q decreases rapidly as a system moves further away from the order−disorder transition (in bulk) or the critical micelle temperature (in solution). While the mechanisms available to self-assembling BCPs have been known in principle and considered for decades, a quantitative understanding of rates in terms of molecular variables is still lacking.

VI.A. Equilibration in Bulk Particle Phases

Issues of metastability and difficulties in forming well-ordered three-dimensional macrolattices are prevalent for BCPs in the bulk. This is particularly true for particle phases, where the system has both a preferred packing symmetry and a preferred Q (or more than a single Q for Frank−Kasper phases). The fact that Q is a function of temperature requires changes in particle number density on heating or cooling, which may be prohibitively slow even when chain exchange is relatively rapid. In contrast, lamellar and cylindrical phases can readily adjust domain spacings without enforced mixing of the two blocks. Further studies in which chain exchange (e.g., by tracer diffusion) and the kinetics of particle phase evolution are both measured on the same system would be highly desirable, in parallel with theoretical studies aimed at describing the mechanisms by which particle number densities can be adjusted.

VI.B. Chain Exchange in Solution

The TR-SANS experiment has provided direct, quantitative access to the rate of chain exchange, as a function of both molecular and micellar variables. Interestingly, the results are systematically different from the expectations of the Halperin−Alexander model. This includes the dependence of the barrier on N_{core}, the sign of the dependence on N_{corona}, and the complete functional dependence on the core−solvent interaction parameter. These issues might best be resolved by simulation, or even by new analytical models. Further experiments, particularly in terms of molecular architecture, micelle morphology, and higher copolymer concentration, would be welcome.

VI.C. Fragmentation in Solution

Measurements of micelle fragmentation for BCPs in ionic liquids have shown (a) a strong dependence on total N, possibly consistent with theory, (b) independence of concentration, as expected, and (c) independence of interfacial tension, suggesting a transition state dictated by corona crowding at a pinch-off point in the neck between two budding fragments. However, measurements across techniques (DLS, SAXS, TEM) reveal a compressed exponential time

https://doi.org/10.1021/acspolymersau.2c00033
ACS Polym. Au 2022, 2, 397−416

dependence, with an Avrami exponent typically *ca.* 2; this observation has not been satisfactorily explained as yet. In these systems, the initial micelles are significantly larger than the equilibrium size ($Q/Q_{eq} > 1.5$), and chain exchange has been shown not to contribute. On the other hand, fluorescence measurements on PEO-PPO-PEO triblocks have accessed information about fragmentation near equilibrium, albeit convoluted with concurrent fusion and chain exchange. The use of liquid-phase TEM offers an opportunity to image the process in real time, if a system with suitably rapid fragmentation can be designed.

VI.D. Fusion in Solution

Although numerous studies have determined that fusion events take place, there have been very few quantitative studies, i.e., those in which fusion rates have been directly related to molecular variables. For high N BCPs and with modest micelle concentrations, one may anticipate vanishingly low rates of fusion. One promising approach could be to prepare micelles with $Q/Q_{eq} < 0.5$, so that fusion becomes a significantly net downhill process (albeit with a significant barrier). This is also a process that is challenging to simulate under realistic conditions, e.g., such that the corona concentration profile is both sufficiently long-ranged and sufficiently dense.

AUTHOR INFORMATION

Corresponding Author

Timothy P. Lodge − *Department of Chemistry, University of Minnesota, Minneapolis, Minnesota 55455, United States; Department of Chemical Engineering & Materials Science, University of Minnesota, Minneapolis, Minnesota 55455, United States;* orcid.org/0000-0001-5916-8834; Email: lodge@umn.edu

Authors

Claire L. Seitzinger − *Department of Chemistry, University of Minnesota, Minneapolis, Minnesota 55455, United States*

Sarah C. Seeger − *Department of Chemical Engineering & Materials Science, University of Minnesota, Minneapolis, Minnesota 55455, United States;* orcid.org/0000-0002-3224-7222

Sanghee Yang − *Department of Chemistry, University of Minnesota, Minneapolis, Minnesota 55455, United States;* orcid.org/0000-0001-7944-6635

Supriya Gupta − *Department of Chemistry, University of Minnesota, Minneapolis, Minnesota 55455, United States*

Kevin D. Dorfman − *Department of Chemical Engineering & Materials Science, University of Minnesota, Minneapolis, Minnesota 55455, United States;* orcid.org/0000-0003-0065-5157

Complete contact information is available at: https://pubs.acs.org/10.1021/acspolymersau.2c00033

Notes

The authors declare no competing financial interest.

ACKNOWLEDGMENTS

This work was supported by the National Science Foundation Polymers Program through Award DMR-2103630. Helpful discussions with Michael Rubinstein, Scott Milner, and Andy Spakowitz are appreciated.

REFERENCES

(1) Gohy, J.-F. Block Copolymer Micelles. *Adv. Polym. Sci.* **2005**, *190*, 65−136.

(2) Mai, Y.; Eisenberg, A. Self-Assembly of Block Copolymers. *Chem. Soc. Rev.* **2012**, *41* (18), 5969−5985.

(3) Tritschler, U.; Pearce, S.; Gwyther, J.; Whittell, G. R.; Manners, I. *50th Anniversary Perspective*: Functional Nanoparticles from the Solution Self-Assembly of Block Copolymers. *Macromolecules* **2017**, *50* (9), 3439−3463.

(4) Atanase, L. I.; Riess, G. Self-Assembly of Block and Graft Copolymers in Organic Solvents: An Overview of Recent Advances. *Polymers* **2018**, *10* (1), 62.

(5) Bates, C. M.; Bates, F. S. *50th Anniversary Perspective*: Block Polymers—Pure Potential. *Macromolecules* **2017**, *50* (1), 3−22.

(6) Leibler, L. Theory of Microphase Separation in Block Copolymers. *Macromolecules* **1980**, *13* (6), 1602−1617.

(7) Matsen, M. W.; Schick, M. Stable and Unstable Phases of a Diblock Copolymer Melt. *Phys. Rev. Lett.* **1994**, *72* (16), 2660−2663.

(8) Arora, A.; Qin, J.; Morse, D. C.; Delaney, K. T.; Fredrickson, G. H.; Bates, F. S.; Dorfman, K. D. Broadly Accessible Self-Consistent Field Theory for Block Polymer Materials Discovery. *Macromolecules* **2016**, *49* (13), 4675−4690.

(9) Fredrickson, G. H. *The Equilibrium Theory of Inhomogeneous Polymers*; Oxford University Press, 2013.

(10) Lee, S.; Bluemle, M. J.; Bates, F. S. Discovery of a Frank-Kasper σ Phase in Sphere-Forming Block Copolymer Melts. *Science* **2010**, *330* (6002), 349−353.

(11) Xie, N.; Li, W.; Qiu, F.; Shi, A.-C. σ Phase Formed in Conformationally Asymmetric AB-Type Block Copolymers. *ACS Macro Lett.* **2014**, *3* (9), 906−910.

(12) Kim, K.; Arora, A.; Lewis, R. M., 3rd; Liu, M.; Li, W.; Shi, A. C.; Dorfman, K. D.; Bates, F. S. Origins of Low-Symmetry Phases in Asymmetric Diblock Copolymer Melts. *Proc. Natl. Acad. Sci. U. S. A.* **2018**, *115* (5), 847−854.

(13) Kim, K.; Schulze, M. W.; Arora, A.; Lewis, R. M., III; Hillmyer, M. A.; Dorfman, K. D.; Bates, F. S. Thermal Processing of Diblock Copolymer Melts Mimics Metallurgy. *Science* **2017**, *356*, 520−523.

(14) Bates, M. W.; Lequieu, J.; Barbon, S. M.; Lewis, R. M., III; Delaney, K. T.; Anastasaki, A.; Hawker, C. J.; Fredrickson, G. H.; Bates, C. M. Stability of the A15 Phase in Diblock Copolymer Melts. *Proc. Natl. Acad. Sci. U. S. A.* **2019**, *116*, 13194−13199.

(15) Noolandi, J.; Hong, K. M. Theory of Block Copolymer Micelles in Solution. *Macromolecules* **1983**, *16* (9), 1443−1448.

(16) Semenov, A. N. Contribution to the Theory of Microphase Layering in Block-Copolymer Melts. *Sov. Phys. JETP* **1985**, *61* (4), 733−742.

(17) Halperin, A. Polymeric Micelles: A Star Model. *Macromolecules* **1987**, *20* (11), 2943−2946.

(18) Halperin, A.; Tirrell, M.; Lodge, T. P. Tethered Chains in Polymer Microstructures. *Adv. Polym. Sci.* **1992**, *100/1*, 31−71.

(19) Nagarajan, R.; Ganesh, K. Block Copolymer Self-Assembly in Selective Solvents: Spherical Micelles with Segregated Cores. *J. Chem. Phys.* **1989**, *90* (10), 5843−5856.

(20) Yuan, X.-F.; Masters, A. J.; Price, C. Self-Consistent Field Theory of Micelle Formation by Block Copolymers. *Macromolecules* **1992**, *25* (25), 6876−6884.

(21) Pépin, M. P.; Whitmore, M. D. Monte Carlo and Mean Field Study of Diblock Copolymer Micelles. *Macromolecules* **2000**, *33* (23), 8644−8653.

(22) Zhulina, E. B.; Adam, M.; LaRue, I.; Sheiko, S. S.; Rubinstein, M. Diblock Copolymer Micelles in a Dilute Solution. *Macromolecules* **2005**, *38* (12), 5330−5351.

(23) Wang, T. Y.; Tsiang, R. C. C.; Liou, J. S.; Wu, J.; Sheu, H. C. Preparation and Characterization of a Star-shaped Polystyrene-*b*-Poly(ethylene-*co*-propylene) Block Copolymer as a Viscosity Index Improver of Lubricant. *J. Appl. Polym. Sci.* **2001**, *79* (10), 1838−1846.

(24) Ge, Z.; Liu, S. Functional Block Copolymer Assemblies Responsive to Tumor and Intracellular Microenvironments for Site-

Specific Drug Delivery and Enhanced Imaging Performance. *Chem. Soc. Rev.* **2013**, *42* (17), 7289−7325.
(25) Elsabahy, M.; Heo, G. S.; Lim, S.-M.; Sun, G.; Wooley, K. L. Polymeric Nanostructures for Imaging and Therapy. *Chem. Rev.* **2015**, *115* (19), 10967−11011.
(26) Monteiro, M. Nanoreactors for Polymerizations and Organic Reactions. *Macromolecules* **2010**, *43* (3), 1159−1168.
(27) Cotanda, P.; Lu, A.; Patterson, J. P.; Petzetakis, N.; O'Reilly, R. K. Functionalized Organocatalytic Nanoreactors: Hydrophobic Pockets for Acylation Reactions in Water. *Macromolecules* **2012**, *45* (5), 2377−2384.
(28) Denkova, A. G.; Mendes, E.; Coppens, M. O. Non-Equilibrium Dynamics of Block Copolymer Micelles in Solution: Recent Insights and Open Questions. *Soft Matter* **2010**, *6* (11), 2351−2357.
(29) Israelachvili, J. N. *Intermolecular and Surface Forces*; Academic Press: London, 1985.
(30) Zana, R. Dynamics in Micellar Solutions of Amphiphilic Block Copolymers. In *Dynamics of Surfactant Self-Assemblies: Micelles, Microemulsions, Vesicles, and Lyotropic Phases*; Hubbard, A. T., Ed.; Taylor & Francis Group/CRC Press: Boca Raton, 2005; pp 161−231.
(31) Rosen, M. J. *Surfactants and Interfacial Phenomena*; Wiley: New York, 1978.
(32) Lindsay, A. P. Ph.D. Thesis; University of Minnesota Twin Cities, 2021.
(33) Aniansson, E. A. G.; Wall, S. N. Kinetics of Step-Wise Micelle Association. *J. Phys. Chem.* **1974**, *78* (10), 1024−1030.
(34) Aniansson, E. A. G.; Wall, S. N. Kinetics of Step-Wise Micelle Association. Correction and Improvement. *J. Phys. Chem.* **1975**, *79* (8), 857−858.
(35) Aniansson, E. A. G.; Wall, S. N.; Almgren, M.; Hoffmann, H.; Kielmann, I.; Ulbricht, W.; Zana, R.; Lang, J.; Tondre, C. Theory of the Kinetics of Micellar Equilibria, and Quantitative Interpretation of Chemical Relaxation Studies of Micellar Solutions of Ionic Surfactants. *J. Phys. Chem.* **1976**, *80* (9), 905−922.
(36) Goldmints, I.; Holzwarth, J. F.; Smith, K. A.; Hatton, T. A. Micellar Dynamics in Aqueous Solutions of PEO-PPO-PEO Block Copolymers. *Langmuir* **1997**, *13* (23), 6130−6134.
(37) Rharbi, Y.; Winnik, M. A.; Hahn, K. G. Kinetics of Fusion and Fragmentation Nonionic Micelles: Triton X-100. *Langmuir* **1999**, *15* (14), 4697−4700.
(38) Rharbi, Y.; Karrouch, M.; Richardson, P. Fusion and Fission Inhibited by the Same Mechanism in Electrostatically Charged Surfactant Micelles. *Langmuir* **2014**, *30* (27), 7947−7952.
(39) Michels, B.; Waton, G.; Zana, R. Dynamics of Micelles of Poly(ethylene oxide)-Poly(propylene oxide)-Poly(ethylene oxide) Block Copolymers in Aqueous Solutions. *Langmuir* **1997**, *13* (12), 3111−3118.
(40) Halperin, A.; Alexander, S. Polymeric Micelles: Their Relaxation Kinetics. *Macromolecules* **1989**, *22* (5), 2403−2412.
(41) Halperin, A. On Micellar Exchange: The Role of the Insertion Penalty. *Macromolecules* **2011**, *44* (13), 5072−5074.
(42) Dormidontova, E. E. Micellization Kinetics in Block Copolymer Solutions: Scaling Model. *Macromolecules* **1999**, *32* (22), 7630−7644.
(43) Nyrkova, I. A.; Semenov, A. N. On the Theory of Micellization Kinetics. *Macromol. Theory Simul.* **2005**, *14* (9), 569−585.
(44) Kahlweit, M.; Teubner, M. On the Kinetics of Micellization in Aqueous Solutions. *Adv. Colloid Interface Sci.* **1980**, *13* (1−2), 1−64.
(45) Aniansson, E. A. G. Theory of Micelle Formation Kinetics. *Ber. Bunsenges. Phys. Chemie* **1978**, *82* (9), 981−988.
(46) Teubner, M. Theory of Ultrasonic Absorption in Micellar Solutions. *J. Phys. Chem.* **1979**, *83* (22), 2917−2920.
(47) Honda, C.; Hasegawa, Y.; Hirunuma, R.; Nose, T. Micellization Kinetics of Block Copolymers in Selective Solvent. *Macromolecules* **1994**, *27* (26), 7660−7668.
(48) Jensen, G. V.; Lund, R.; Gummel, J.; Monkenbusch, M.; Narayanan, T.; Pedersen, J. S. Direct Observation of the Formation of Surfactant Micelles under Nonisothermal Conditions by Synchrotron SAXS. *J. Am. Chem. Soc.* **2013**, *135* (19), 7214−7222.
(49) Lund, R.; Willner, L.; Monkenbusch, M.; Panine, P.; Narayanan, T.; Colmenero, J.; Richter, D. Structural Observation and Kinetic Pathway in the Formation of Polymeric Micelles. *Phys. Rev. Lett.* **2009**, *102* (18), 188301.
(50) Kresheck, G. C.; Hamori, E.; Davenport, G.; Scheraga, H. A. Determination of the Dissociation Rate of Dodecylpyridinium Iodide Micelles by a Temperature-Jump Technique. *J. Am. Chem. Soc.* **1966**, *88* (2), 246−253.
(51) He, Y.; Li, Z.; Simone, P.; Lodge, T. P. Self-Assembly of Block Copolymer Micelles in an Ionic Liquid. *J. Am. Chem. Soc.* **2006**, *128* (8), 2745−2750.
(52) Choi, S.; Bates, F. S.; Lodge, T. P. Small-Angle X-ray Scattering of Concentration Dependent Structures in Block Copolymer Solutions. *Macromolecules* **2014**, *47* (22), 7978−7986.
(53) Lodge, T. P.; Bang, J.; Hanley, K. J.; Krocak, J.; Dahlquist, S.; Sujan, B.; Ott, J. The Origins of Anomalous Micellization in Diblock Copolymer Solutions. *Langmuir* **2003**, *19* (6), 2103−2109.
(54) Hoarfrost, M. L.; Lodge, T. P. Effects of Solvent Quality and Degree of Polymerization on the Critical Micelle Temperature of Poly(ethylene oxide-*b*-n-butyl methacrylate) in Ionic Liquids. *Macromolecules* **2014**, *47* (4), 1455−1461.
(55) Lodge, T. P.; Bang, J.; Park, M. J.; Char, K. Origin of the Thermoreversible fcc/bcc Transition in Block Copolymer Solutions. *Phys. Rev. Lett.* **2004**, *92*, 145501.
(56) Bang, J.; Viswanathan, K.; Lodge, T. P.; Park, M.-J.; Char, K. Temperature Dependent Micellar Structures in Poly(styrene-*b*-isoprene) Diblock Copolymer Solutions Near the Critical Micelle Temperature. *J. Chem. Phys.* **2004**, *121* (22), 11489.
(57) Dalvi, M. C.; Lodge, T. P. Parallel and Perpendicular Chain Diffusion in a Lamellar Block Copolymer. *Macromolecules* **1993**, *26* (4), 859−861.
(58) Dalvi, M. C.; Eastman, C. E.; Lodge, T. P. Diffusion in Microstructured Block Copolymers: Chain Localization and Entanglements. *Phys. Rev. Lett.* **1993**, *71* (16), 2591.
(59) Dalvi, M. C.; Lodge, T. P. Diffusion in Block Copolymer Melts: The Disordered Region and the Vicinity of the Order-Disorder Transition. *Macromolecules* **1994**, *27* (13), 3487−3492.
(60) Dalvi, M. C.; Lodge, T. P. Mechanisms of Chain Diffusion in Lamellar Block Copolymers. *Phys. Rev. Lett.* **1995**, *75* (4), 657.
(61) Hamersky, M. W.; Tirrell, M.; Lodge, T. P. Self-Diffusion of a Polystyrene-Polyisoprene Block Copolymer. *J. Polym. Sci., Polym. Phys. Ed.* **1996**, *34* (17), 2899−2909.
(62) Yokoyama, H.; Kramer, E. J. Self-Diffusion of Asymmetric Diblock Copolymers with a Spherical Domain Structure. *Macromolecules* **1998**, *31* (22), 7871−7876.
(63) Hamersky, M. W.; Hillmyer, M. A.; Tirrell, M.; Bates, F. S.; Lodge, T. P.; von Meerwall, E. D. Block Copolymer Self-Diffusion in the Gyroid and Cylinder Morphologies. *Macromolecules* **1998**, *31* (16), 5363−5370.
(64) Yokoyama, H.; Kramer, E. J.; Fredrickson, G. H. Simulation of Diffusion of Asymmetric Diblock and Triblock Copolymers in a Spherical Domain Structure. *Macromolecules* **2000**, *33* (6), 2249−2257.
(65) Cavicchi, K. A.; Lodge, T. P. Domain Size Equilibration in Sphere-forming Block Copolymers. *J. Polym. Sci., Polym. Phys. Ed.* **2003**, *41* (7), 715−724.
(66) Cavicchi, K. A.; Lodge, T. P. Self and Tracer Diffusion in Sphere-forming Block Copolymers. *Macromolecules* **2003**, *36* (19), 7158−7164.
(67) Cavicchi, K. A.; Lodge, T. P. Anisotropic Self-Diffusion in Block Copolymer Cylinders. *Macromolecules* **2004**, *37* (16), 6004−6012.
(68) Helfand, E. Diffusion in Strongly Segregated Block Copolymers. *Macromolecules* **1992**, *25* (1), 492−493.
(69) Balagurusamy, V. S. K.; Ungar, G.; Percec, V.; Johansson, G. Rational Design of the First Spherical Supramolecular Dendrimers Self-Organized in a Novel Thermotropic Cubic Liquid-Crystalline Phase and the Determination of Their Shape by X-Ray Analysis. *J. Am. Chem. Soc.* **1997**, *119* (7), 1539−1555.

https://doi.org/10.1021/acspolymersau.2c00033
ACS Polym. Au 2022, 2, 397−416

(70) Yue, K.; Huang, M.; Marson, R. L.; He, J.; Huang, J.; Zhou, Z.; Wang, J.; Liu, C.; Yan, X.; Wu, K.; Guo, Z.; Liu, H.; Zhang, W.; Ni, P.; Wesdemiotis, C.; Zhang, W.-B.; Glotzer, S. C.; Cheng, S. Z. D. Geometry Induced Sequence of Nanoscale Frank-Kasper and Quasicrystal Mesophases in Giant Surfactants. *Proc. Natl. Acad. Sci. U.S.A.* **2016**, *113* (50), 14195−14200.
(71) Gillard, T. M.; Lee, S.; Bates, F. S. Dodecagonal Quasicrystalline Order in a Diblock Copolymer Melt. *Proc. Natl. Acad. Sci. U.S.A.* **2016**, *113* (19), 5167−5172.
(72) Baez-Cotto, C. M.; Mahanthappa, M. K. Micellar Mimicry of Intermetallic C14 and C15 Laves Phases by Aqueous Lyotropic Self-Assembly. *ACS Nano* **2018**, *12* (4), 3226−3234.
(73) Bates, M. W.; Lequieu, J.; Barbon, S. M.; Lewis, R. M.; Delaney, K. T.; Anastasaki, A.; Hawker, C. J.; Fredrickson, G. H.; Bates, C. M. Stability of the A15 Phase in Diblock Copolymer Melts. *Proc. Natl. Acad. Sci. U.S.A.* **2019**, *116* (27), 13194−13199.
(74) Lindsay, A. P.; Jayaraman, A.; Peterson, A. J.; Mueller, A. J.; Weigand, S. J.; Almdal, K.; Mahanthappa, M.; Lodge, T. P.; Bates, F. S. Reevaluation of Poly(ethylene-*alt*-propylene)-*block*-Polydimethylsiloxane Phase Behavior Uncovers Topological Close-Packing and Epitaxial Quasicrystal Growth. *ACS Nano* **2021**, *15* (6), 9453−9468.
(75) Lang, J.; Tondre, C.; Zana, R.; Bauer, R.; Hoffmann, H.; Ulbricht, W. Chemical Relaxation Studies of Micellar Equilibriums. *J. Phys. Chem.* **1975**, *79* (3), 276−283.
(76) Lessner, E.; Teubner, M.; Kahlweit, M. Relaxation Experiments in Aqueous Solutions of Ionic Micelles: 2. Experiments on the System Water-Sodium Dodecyl Sulfate-Sodium Perchlorate and their Theoretical Interpretation. *J. Phys. Chem.* **1981**, *85* (21), 3167−3175.
(77) Kahlweit, M. Kinetics of Formation of Association Colloids. *J. Colloid Interface Sci.* **1982**, *90* (1), 92−99.
(78) Rharbi, Y.; Chen, L.; Winnik, M. A. Exchange Mechanisms for Sodium Dodecyl Sulfate Micelles: High Salt Concentration. *J. Am. Chem. Soc.* **2004**, *126* (19), 6025−6034.
(79) Frindi, M.; Michels, B.; Zana, R. Ultrasonic Absorption Studies of Surfactant Exchange Between Micelles and Bulk Phase in Aqueous Micellar Solutions of Nonionic Surfactants with a Short Alkyl Chain. 3. Surfactants with a Sugar Head Group. *J. Phys. Chem.* **1992**, *96* (20), 8137−8141.
(80) Jensen, G. V.; Lund, R.; Narayanan, T.; Pedersen, J. S. Transformation from Globular to Cylindrical Mixed Micelles through Molecular Exchange that Induces Micelle Fusion. *J. Phys. Chem. Lett.* **2016**, *7* (11), 2039−2043.
(81) Maillet, J. B.; Lachet, V.; Coveney, P. V. Large Scale Molecular Dynamics Simulation of Self-Assembly Processes in Short and Long Chain Cationic Surfactants. *Phys. Chem. Chem. Phys.* **1999**, *1* (23), 5277−5290.
(82) Hadgiivanova, R.; Diamant, H.; Andelman, D. Kinetics of Surfactant Micellization: A Free Energy Approach. *J. Phys. Chem. B* **2011**, *115* (22), 7268−7280.
(83) Wang, Y.; Balaji, R.; Quirk, R. P.; Mattice, W. L. Detection of the Rate of Exchange of Chains between Micelles Formed by Diblock Copolymers in Aqueous Solution. *Polym. Bull.* **1992**, *28*, 333−338.
(84) Cao, T.; Munk, P.; Ramireddy, C.; Tuzar, Z.; Webber, S. E. Fluorescence Studies of Amphiphilic Poly(Methacrylic Acid)-Block-Polystyrene-Block-Poly(Methacrylic Acid) Micelles. *Macromolecules* **1991**, *24* (23), 6300−6305.
(85) Smith, C. K.; Liu, G. Determination of the Rate Constant for Chain Insertion into Poly(Methyl Methacrylate)-*Block*-Poly-(Methacrylic Acid) Micelles by a Fluorescence Method. *Macromolecules* **1996**, *29* (6), 2060−2067.
(86) Wang, Y.; Kausch, C. M.; Chun, M.; Quirk, R. P.; Mattice, W. L. Exchange of Chains between Micelles of Labeled Polystyrene-Block-Poly(Oxyethylene) As Monitored by Nonradiative Singlet Energy Transfer. *Macromolecules* **1995**, *28* (4), 904−911.
(87) Prochazka, K.; Bednar, B.; Mukhtar, E.; Svoboda, P.; Trnena, J.; Almgren, M. Nonradiative Energy Transfer in Block Copolymer Micelles. *J. Phys. Chem.* **1991**, *95* (11), 4563−4568.
(88) Creutz, S.; van Stam, J.; Antoun, S.; De Schryver, F. C.; Jerome, R. Exchange of Polymer Molecules between Block Copolymer Micelles Studied by Emission Spectroscopy. A Method for the Quantification of Unimer Exchange Rates. *Macromolecules* **1997**, *30* (14), 4078−4083.
(89) Creutz, S.; van Stam, J.; de Schryver, F. C.; Jérôme, R. Dynamics of Poly((Dimethylamino)Alkyl Methacrylate-Block-Sodium Methacrylate) Micelles. Influence of Hydrophobicity and Molecular Architecture on the Exchange Rate of Copolymer Molecules. *Macromolecules* **1998**, *31* (3), 681−689.
(90) Underhill, R. S.; Ding, J.; Birss, V. I.; Liu, G. Chain Exchange Kinetics of Polystyrene- *Block* -Poly(2-Cinnamoylethyl Methacrylate) Micelles in THF/Cyclopentane Mixtures. *Macromolecules* **1997**, *30* (26), 8298−8303.
(91) Rager, T.; Meyer, W. H.; Wegner, G. Micelle Formation of Poly(acrylic acid)-*block*-Poly(methyl methacrylate) Block Copolymers in Mixtures of Water with Organic Solvents. *Macromol. Chem. Phys.* **1999**, *200* (7), 1672−1680.
(92) van Stam, J.; Creutz, S.; De Schryver, F. C.; Jérôme, R. Tuning of the Exchange Dynamics of Unimers between Block Copolymer Micelles with Temperature, Cosolvents, and Cosurfactants. *Macromolecules* **2000**, *33* (17), 6388−6395.
(93) Willner, L.; Poppe, A.; Allgaier, J.; Monkenbusch, M.; Richter, D. Time-resolved SANS for the Determination of Unimer Exchange Kinetics in Block Copolymer Micelles. *Europhys. Lett.* **2001**, *55* (5), 667−673.
(94) Won, Y.-Y.; Davis, H. T.; Bates, F. S. Molecular Exchange in PEO−PB Micelles in Water. *Macromolecules* **2003**, *36* (3), 953−955.
(95) Ma, Y.; Lodge, T. P. Chain Exchange Kinetics in Diblock Copolymer Micelles in Ionic Liquids: The Role of χ. *Macromolecules* **2016**, *49* (24), 9542−9552.
(96) Lund, R.; Willner, L.; Richter, D.; Dormidontova, E. E. Equilibrium Chain Exchange Kinetics of Diblock Copolymer Micelles: Tuning and Logarithmic Relaxation. *Macromolecules* **2006**, *39* (13), 4566−4575.
(97) Lu, J.; Bates, F. S.; Lodge, T. P. Remarkable Effect of Molecular Architecture on Chain Exchange in Triblock Copolymer Micelles. *Macromolecules* **2015**, *48* (8), 2667−2676.
(98) Choi, S.; Lodge, T. P.; Bates, F. S. Mechanism of Molecular Exchange in Diblock Copolymer Micelles: Hypersensitivity to Core Chain Length. *Phys. Rev. Lett.* **2010**, *104* (4), 047802.
(99) Zinn, T.; Willner, L.; Pipich, V.; Richter, D.; Lund, R. Equilibrium Exchange Kinetics in n-alkyl−PEO Polymeric Micelles: Single Exponential Relaxation and Chain Length Dependence. *Soft Matter* **2012**, *8* (3), 623−626.
(100) Zinn, T.; Willner, L.; Lund, R.; Pipich, V.; Richter, D. Molecular Exchange Kinetics of Micelles: Corona Chain Length Dependence. *ACS Macro Lett.* **2016**, *5* (7), 884−888.
(101) Wang, E.; Lu, J.; Bates, F. S.; Lodge, T. P. Effect of Corona Block Length on the Structure and Chain Exchange Kinetics of Block Copolymer Micelles. *Macromolecules* **2018**, *51* (10), 3563−3571.
(102) Wang, E.; Zhu, J.; Zhao, D.; Xie, S.; Bates, F. S.; Lodge, T. P. Effect of Solvent Selectivity on Chain Exchange Kinetics in Block Copolymer Micelles. *Macromolecules* **2020**, *53* (1), 417−426.
(103) Choi, S.-H.; Bates, F. S.; Lodge, T. P. Molecular Exchange in Ordered Diblock Copolymer Micelles. *Macromolecules* **2011**, *44* (9), 3594−3604.
(104) Lu, J.; Bates, F. S.; Lodge, T. P. Addition of Corona Block Homopolymer Retards Chain Exchange in Solutions of Block Copolymer Micelles. *Macromolecules* **2016**, *49* (4), 1405−1413.
(105) Zhao, D.; Ma, Y.; Lodge, T. P. Exchange Kinetics for a Single Block Copolymer in Micelles of Two Different Sizes. *Macromolecules* **2018**, *51* (6), 2312−2320.
(106) Lund, R.; Willner, L.; Pipich, V.; Grillo, I.; Lindner, P.; Colmenero, J.; Richter, D. Equilibrium Chain Exchange Kinetics of Diblock Copolymer Micelles: Effect of Morphology. *Macromolecules* **2011**, *44* (15), 6145−6154.
(107) Lu, J.; Bates, F. S.; Lodge, T. P. Remarkable Effect of Molecular Architecture on Chain Exchange in Triblock Copolymer Micelles. *Macromolecules* **2015**, *48* (8), 2667−2676.

https://doi.org/10.1021/acspolymersau.2c00033
ACS Polym. Au 2022, 2, 397−416

(108) Balsara, N. P.; Tirrell, M.; Lodge, T. P. Micelle Formation of BAB Triblock Copolymers in Solvents that Preferentially Dissolve the A Block. *Macromolecules* **1991**, *24* (8), 1975−1986.
(109) Peters, A. J.; Lodge, T. P. Comparison of Gel Relaxation Times and End-block Pullout Times in ABA Triblock Copolymer Networks. *Macromolecules* **2016**, *49* (19), 7340−7349.
(110) Kim, S.; Lee, S.; Choi, S.-H.; Char, K. Chain Exchange Kinetics of Bottlebrush Block Copolymer Micelles. *Macromolecules* **2021**, *54* (10), 4739−4746.
(111) Groot, R. D.; Warren, P. B. Dissipative Particle Dynamics: Bridging the Gap between Atomistic and Mesoscopic Simulation. *J. Chem. Phys.* **1997**, *107* (11), 4423−4435.
(112) Li, Z.; Dormidontova, E. E. Kinetics of Diblock Copolymer Micellization by Dissipative Particle Dynamics. *Macromolecules* **2010**, *43* (7), 3521−3531.
(113) Li, Z.; Dormidontova, E. E. Equilibrium Chain Exchange Kinetics in Block Copolymer Micelle Solutions by Dissipative Particle Dynamics Simulations. *Soft Matter* **2011**, *7* (9), 4179.
(114) Seeger, S. C.; Dorfman, K. D.; Lodge, T. P. Free Energy Trajectory for Escape of a Single Chain from a Diblock Copolymer Micelle. *ACS Macro Lett.* **2021**, *10*, 1570−1575.
(115) Prhashanna, A.; Khan, S. A.; Chen, S. B. Kinetics of Chain Exchange between Diblock Copolymer Micelles. *Macromol. Theory Simul.* **2016**, *25* (4), 383−391.
(116) Prhashanna, A.; Chen, S. B. Chain Exchange Kinetics between Linear ABA-Type Triblock Copolymer Micelles. *Polymer* **2017**, *118*, 22−29.
(117) Peters, A. J.; Lodge, T. P. Chain Exchange Kinetics of Asymmetric B_1AB_2 Linear Triblock and AB_1B_2 Branched Triblock Copolymers. *Macromolecules* **2017**, *50* (16), 6303−6313.
(118) Prhashanna, A.; Dormidontova, E. E. Tadpole and Mixed Linear/Tadpole Micelles of Diblock Copolymers: Thermodynamics and Chain Exchange Kinetics. *Macromolecules* **2017**, *50* (4), 1740−1748.
(119) Prhashanna, A.; Dormidontova, E. E. Micelle Self-Assembly and Chain Exchange Kinetics of Tadpole Block Copolymers with a Cyclic Corona Block. *Macromolecules* **2020**, *53* (3), 982−991.
(120) Guo, J.; Liang, H.; Wang, Z. G. Coil-to-Globule Transition by Dissipative Particle Dynamics Simulation. *J. Chem. Phys.* **2011**, *134* (24), 244904−244904.
(121) Ye, X.; Khomami, B. Self-Assembly of Linear Diblock Copolymers in Selective Solvents: From Single Micelles to Particles with Tri-Continuous Inner Structures. *Soft Matter* **2020**, *16* (26), 6056.
(122) Torrie, G. M.; Valleau, J. P. Nonphysical Sampling Distributions in Monte Carlo Free-Energy Estimation: Umbrella Sampling. *J. Comput. Phys.* **1977**, *23* (2), 187−199.
(123) Chodera, J. D.; Swope, W. C.; Pitera, J. W.; Seok, C.; Dill, K. A. Use of the Weighted Histogram Analysis Method for the Analysis of Simulated and Parallel Tempering Simulations. *J. Chem. Theory Comput.* **2007**, *3* (1), 26−41.
(124) Yuan, F.; Wang, S.; Larson, R. G. Potentials of Mean Force and Escape Times of Surfactants from Micelles and Hydrophobic Surfaces Using Molecular Dynamics Simulations. *Langmuir* **2015**, *31* (4), 1336−1343.
(125) Mysona, J. A.; McCormick, A. V.; Morse, D. C. Mechanism of Micelle Birth and Death. *Phys. Rev. Lett.* **2019**, *123* (3), 038003.
(126) Mysona, J. A.; McCormick, A. V.; Morse, D. C. Simulation of Diblock Copolymer Surfactants. I. Micelle Free Energies. *Phys. Rev. E* **2019**, *100* (1), 012602.
(127) Mysona, J. A.; McCormick, A. V.; Morse, D. C. Simulation of Diblock Copolymer Surfactants. II. Micelle Kinetics. *Phys. Rev. E* **2019**, *100* (1), 012603.
(128) García Daza, F. A.; Avalos, J. B.; Mackie, A. D. Simulation Analysis of the Kinetic Exchange of Copolymer Surfactants in Micelles. *Langmuir* **2017**, *33* (27), 6794−6803.
(129) García Daza, F. A.; Bonet Avalos, J.; Mackie, A. D. Logarithmic Exchange Kinetics in Monodisperse Copolymeric Micelles. *Phys. Rev. Lett.* **2017**, *118* (24), 248001.
(130) Pantelidou, M. S.; García Daza, F. A.; Avalos, J. B.; Mackie, A. D. Universal Scaling for the Exit Dynamics of Block Copolymers from Micelles at Short and Long Time Scales. *Macromolecules* **2022**, *55* (3), 914−927.
(131) Giacomello, M.; Pyakurel, A.; Glytsou, C.; Scorrano, L. The Cell Biology of Mitochondrial Membrane Dynamics. *Nat. Rev. Mol. Cell Biol.* **2020**, *21*, 204−224.
(132) Chernomordik, L. V.; Kozlov, M. M. Protein-Lipid Interplay in Fusion and Fission of Biological Membranes. *Annu. Rev. Biochem.* **2003**, *72*, 175−207.
(133) Tahir, M. A.; Guven, Z. P.; Arriaga, L. R.; Tinao, B.; Yang, Y.-S. S.; Bekdemir, A.; Martin, J. T.; Bhanji, A. N.; Irvine, D.; Stellacci, F.; Alexander-Katz, A. Calcium-triggered fusion of lipid membranes is enabled by amphiphilic nanoparticles. *Proc. Natl. Acad. Sci. U. S. A.* **2020**, *117* (31), 18470−18476.
(134) Zana, R.; Weill, C. Effect of Temperature on the Aggregation Behaviour of Nonionic Surfactants in Aqueous Solutions. *J. Phys., Lett.* **1985**, *46* (20), 953−960.
(135) Rharbi, Y.; Li, M.; Winnik, M. A.; Hahn, K. G. Temperature Dependence of Fusion and Fragmentation Kinetics of Triton X-100 Micelles. *J. Am. Chem. Soc.* **2000**, *122* (26), 6242−6251.
(136) Rharbi, Y.; Winnik, M. A. Salt Effects on Solute Exchange and Micelle Fission in Sodium Dodecyl Sulfate Micelles below the Micelle-to-Rod Transition. *J. Phys. Chem. B* **2003**, *107* (7), 1491−1501.
(137) Menger, F. M.; Balachander, N. Chemically-induced Aggregation, Budding, and Fusion in Giant Vesicles: Direct Observation by Light Microscopy. *J. Am. Chem. Soc.* **1992**, *114* (14), 5862−5863.
(138) Pool, R.; Bolhuis, P. G. Sampling the Kinetic Pathways of a Micelle Fusion and Fission Transition. *J. Chem. Phys.* **2007**, *126* (24), 244703.
(139) Sammalkorpi, M.; Karttunen, M.; Haataja, M. Micelle Fission through Surface Instability and Formation of an Interdigitating Stalk. *J. Am. Chem. Soc.* **2008**, *130* (52), 17977−17980.
(140) Li, S. Y.; Zhang, X. R.; Dong, W.; Wang, W. C. Computer Simulations of Solute Exchange Using Micelles by a Collision-Driven Fusion Process. *Langmuir* **2008**, *24* (17), 9344−9353.
(141) Gao, J.; Li, S.; Zhang, X.; Wang, W. Computer Simulations of Micelle Fission. *Phys. Chem. Chem. Phys.* **2010**, *12* (13), 3219−3228.
(142) Ghosh, R.; Satarifard, V.; Grafmüller, A.; Lipowsky, R. Budding and Fission of Nanovesicles Induced by Membrane Adsorption of Small Solutes. *ACS Nano* **2021**, *15* (4), 7237−7248.
(143) Rharbi, Y. Fusion and Fragmentation Dynamics at Equilibrium in Triblock Copolymer Micelles. *Macromolecules* **2012**, *45* (24), 9823−9826.
(144) Landazuri, G.; Fernandez, V. V. A.; Soltero, J. F. A.; Rharbi, Y. Length of the Core Forming Block Effect on Fusion and Fission Dynamics at Equilibrium in PEO-PPO-PEO Triblock Copolymer Micelles in the Spherical Regime. *Macromolecules* **2021**, *54* (5), 2494−2505.
(145) Kelley, E. G.; Murphy, R. P.; Seppala, J. E.; Smart, T. P.; Hann, S. D.; Sullivan, M. O.; Epps, T. H. Size Evolution of Highly Amphiphilic Macromolecular Solution Assemblies via a Distinct Bimodal Pathway. *Nat. Commun.* **2014**, *5*, 3599.
(146) Murphy, R. P.; Kelley, E. G.; Rogers, S. A.; Sullivan, M. O.; Epps, T. H. Unlocking Chain Exchange in Highly Amphiphilic Block Polymer Micellar Systems: Influence of Agitation. *ACS Macro Lett.* **2014**, *3* (11), 1106−1111.
(147) Zhou, Y.; Yan, D. Real-Time Membrane Fusion of Giant Polymer Vesicles. *J. Am. Chem. Soc.* **2005**, *127* (30), 10468−10469.
(148) Parent, L. R.; Bakalis, E.; Ramírez-Hernández, A.; Kammeyer, J. K.; Park, C.; de Pablo, J.; Zerbetto, F.; Patterson, J. P.; Gianneschi, N. C. Directly Observing Micelle Fusion and Growth in Solution by Liquid-Cell Transmission Electron Microscopy. *J. Am. Chem. Soc.* **2017**, *139* (47), 17140−17151.
(149) Meli, L.; Santiago, J. M.; Lodge, T. P. Path-Dependent Morphology and Relaxation Kinetics of Highly Amphiphilic Diblock

Copolymer Micelles in Ionic Liquids. *Macromolecules* **2010**, *43* (4), 2018−2027.
(150) Meli, L.; Lodge, T. P. Equilibrium vs Metastability: High-Temperature Annealing of Spherical Block Copolymer Micelles in an Ionic Liquid. *Macromolecules* **2009**, *42* (3), 580−583.
(151) Early, J. T.; Yager, K. G.; Lodge, T. P. Direct Observation of Micelle Fragmentation via In Situ Liquid-Phase Transmission Electron Microscopy. *ACS Macro Lett.* **2020**, *9* (5), 756−761.
(152) Early, J. T.; Lodge, T. P. Fragmentation of 1,2-Polybutadiene-block-Poly(ethylene oxide) Micelles in Imidazolium-Based Ionic Liquids. *Macromolecules* **2019**, *52* (18), 7089−7101.
(153) Early, J. T.; Block, A.; Yager, K. G.; Lodge, T. P. Molecular Weight Dependence of Block Copolymer Micelle Fragmentation Kinetics. *J. Am. Chem. Soc.* **2021**, *143* (20), 7748−7758.
(154) Ryu, C. Y.; Lodge, T. P. Thermodynamic Stability and Anisotropic Fluctuations in the Cylinder-to-Sphere Transition of a Block Copolymer. *Macromolecules* **1999**, *32*, 7190.
(155) Abbas, S.; Li, Z.; Hassan, H.; Lodge, T. P. Thermoreversible Morphology Transitions of Poly(styrene-*b*-dimethylsiloxane) Diblock Copolymer Micelles in Dilute Solution. *Macromolecules* **2007**, *40*, 4048−4052.
(156) Landazuri, G.; Fernandez, V. V. A.; Soltero, J. F. A.; Rharbi, Y. Kinetics of the Sphere-to-Rod like Micelle Transition in a Pluronic Triblock Copolymer. *J. Phys. Chem. B* **2012**, *116* (38), 11720−11727.
(157) Cornel, E. J.; O'Hora, P. S.; Smith, T.; Growney, D. J.; Mykhaylyk, O. O.; Armes, S. P. SAXS Studies of the Thermally-induced Fusion of Diblock Copolymer Spheres: Formation of Hybrid Nanoparticles of Intermediate Size and Shape. *Chem. Sci.* **2020**, *11* (17), 4312−4321.
(158) Lund, R.; Willner, L.; Richter, D.; Lindner, P.; Narayanan, T. Kinetic Pathway of the Cylinder-to-Sphere Transition in Block Copolymer Micelles Observed in Situ by Time-Resolved Neutron and Synchrotron Scattering. *ACS Macro Lett.* **2013**, *2* (12), 1082−1087.

https://doi.org/10.1021/acspolymersau.2c00033
ACS Polym. Au 2022, 2, 397−416